Characterisation of Novel Functional Materials via Neutron Scattering

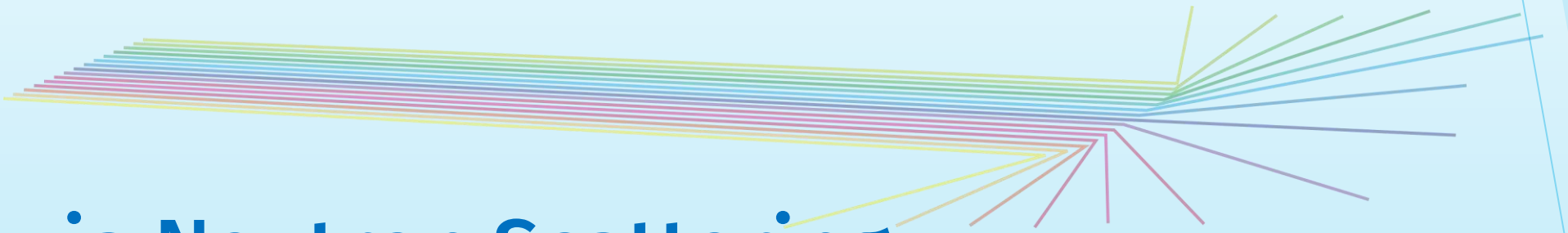

Wojciech Zając

THE HENRYK NIEWODNICZAŃSKI
INSTITUTE OF NUCLEAR PHYSICS
POLISH ACADEMY OF SCIENCES

1


PAUL SCHERRER INSTITUT
PSI
neutron imaging & activation group
©

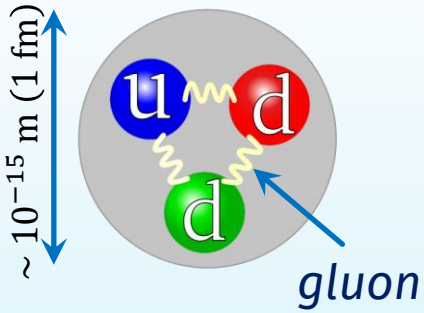

The neutron

Quantity	Symbol	Value
Rest mass	m_n	$1.674927211(84) \times 10^{-27}$ kg
		1.00866491597(43) at.u.
	$m_n c^2$	939.565346(23) MeV
Spin	I	½
Charge		0
Magnetic moment	μ_n	$-0.96623641 \cdot 10^{-27}$ J·T
		$-1.04187565 \cdot 10^{-3}\ \mu_B$
		$-1.91304276\ \mu_N$
Mean life time (free)	τ	879.9±0.9 s (very recent value)

Spin and magnetic moment are oppositely oriented, complicating what "up" and "down" mean with respect to an applied field.

X-rays and neutron attenuation coefficients

Attenuation coefficients with X-ray [cm?¹]

1a	2a	3b	4b	5b	6b	7b	8			1b	2b	3a	4a	5a	6a	7a	0
H 0.02																	He 0.02
Li 0.06	Be 0.22											B 0.28	C 0.27	N 0.11	O 0.16	F 0.14	Ne 0.17
Na 0.13	Mg 0.24											Al 0.38	Si 0.33	P 0.25	S 0.30	Cl 0.23	Ar 0.20
K 0.14	Ca 0.26	Sc 0.48	Ti 0.73	V 1.04	Cr 1.29	Mn 1.32	Fe 1.57	Co 1.78	Ni 1.96	Cu 1.97	Zn 1.64	Ga 1.42	Ge 1.33	As 1.50	Se 1.23	Br 0.90	Kr 0.73
Rb 0.47	Sr 0.86	Y 1.61	Zr 2.47	Nb 3.43	Mo 4.29	Tc 5.06	Ru 5.71	Rh 6.08	Pd 6.13	Ag 5.67	Cd 4.84	In 4.31	Sn 3.98	Sb 4.28	Te 4.06	I 3.45	Xe 2.53
Cs 1.42	Ba 2.73	La 5.04	Hf 19.70	Ta 25.47	W 30.49	Re 34.47	Os 37.92	Ir 39.01	Pt 38.61	Au 35.94	Hg 25.88	Tl 23.23	Pb 22.81	Bi 20.28	Po 20.22	At	Rn 9.77
Fr	Ra 11.80	Ac 24.47	Rf	Ha													

Lanthanides	Ce 5.79	Pr 6.23	Nd 6.46	Pm 7.33	Sm 7.68	Eu 5.66	Gd 8.69	Tb 9.46	Dy 10.17	Ho 10.91	Er 11.70	Tm 12.49	Yb 9.32	Lu 14.07
*Actinides	Th 28.95	Pa 39.65	U 49.08	Np	Pu	Am	Cm	Bk	Vf	Es	Fm	Md	No	Lr x-ray

For X-rays = proportional increase!

Attenuation coefficients with neutrons [cm?¹]

1a	2a	3b	4b	5b	6b	7b	8			1b	2b	3a	4a	5a	6a	7a	0
H 3.44																	He 0.02
Li 3.30	Be 0.79											B 101.60	C 0.56	N 0.43	O 0.17	F 0.20	Ne 0.10
Na 0.09	Mg 0.15											Al 0.10	Si 0.11	P 0.12	S 0.06	Cl 1.33	Ar 0.03
K 0.06	Ca 0.08	Sc 2.00	Ti 0.60	V 0.72	Cr 0.54	Mn 1.21	Fe 1.19	Co 3.92	Ni 2.05	Cu 1.07	Zn 0.35	Ga 0.49	Ge 0.47	As 0.67	Se 0.73	Br 0.24	Kr 0.61
Rb 0.08	Sr 0.14	Y 0.27	Zr 0.29	Nb 0.40	Mo 0.52	Tc 1.76	Ru 0.58	Rh 10.88	Pd 0.78	Ag 4.04	Cd 115.11	In 7.58	Sn 0.21	Sb 0.30	Te 0.25	I 0.23	Xe 0.43
Cs 0.29	Ba 0.07	La 0.52	Hf 4.99	Ta 1.49	W 1.47	Re 6.85	Os 2.24	Ir 30.46	Pt 1.46	Au 6.23	Hg 16.21	Tl 0.47	Pb 0.38	Bi 0.27	Po	At	Rn
Fr	Ra 0.34	Ac	Rf	Ha													

*Lanthanides	Ce 0.14	Pr 0.41	Nd 1.87	Pm 5.72	Sm 171.47	Eu 94.58	Gd 1479.04	Tb 0.93	Dy 32.42	Ho 2.25	Er 5.48	Tm 3.53	Yb 1.40	Lu 2.75
**Actinides	Th 0.59	Pa 8.46	U 0.82	Np 9.80	Pu 50.20	Am 2.86	Cm	Bk	Cf	Es	Fm	Md	No	Lr neut.

For neutrons = completely unsystematic!

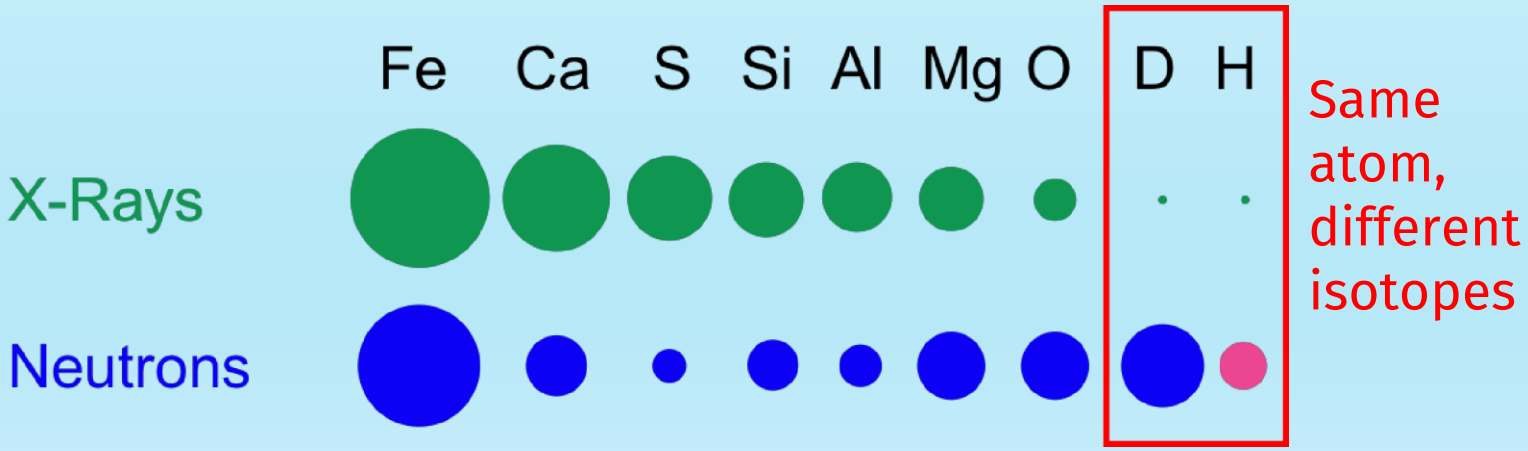

Absorption vs. Scattering

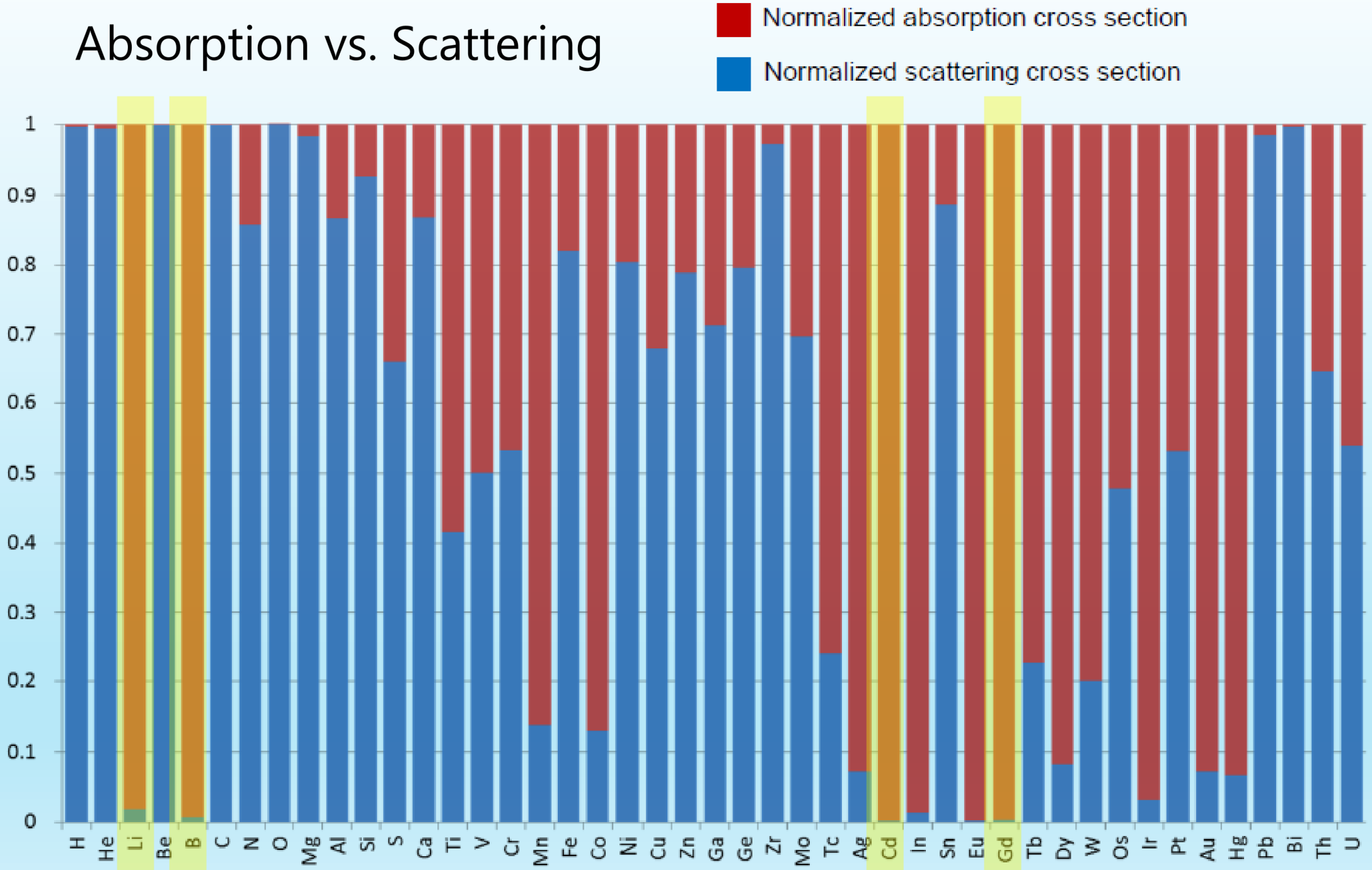

Reconstructed ferritic structure

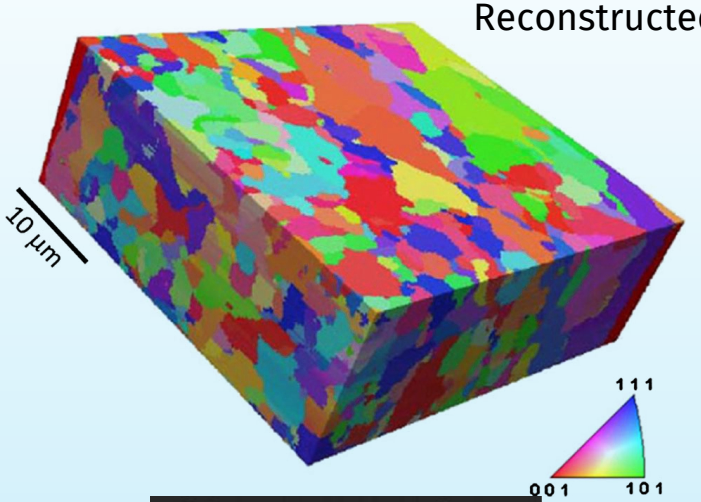

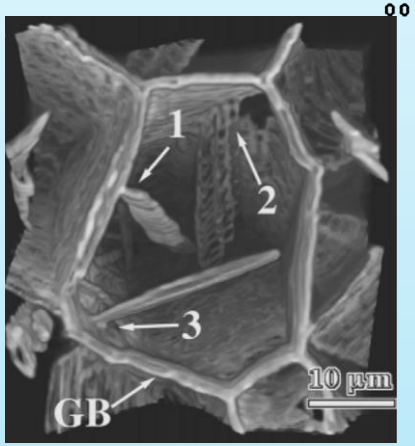

Image of proeutectoid cementite

Graphical representation of the resolution and typical volume analysed per experiment for modern tomographic characterisation methods.

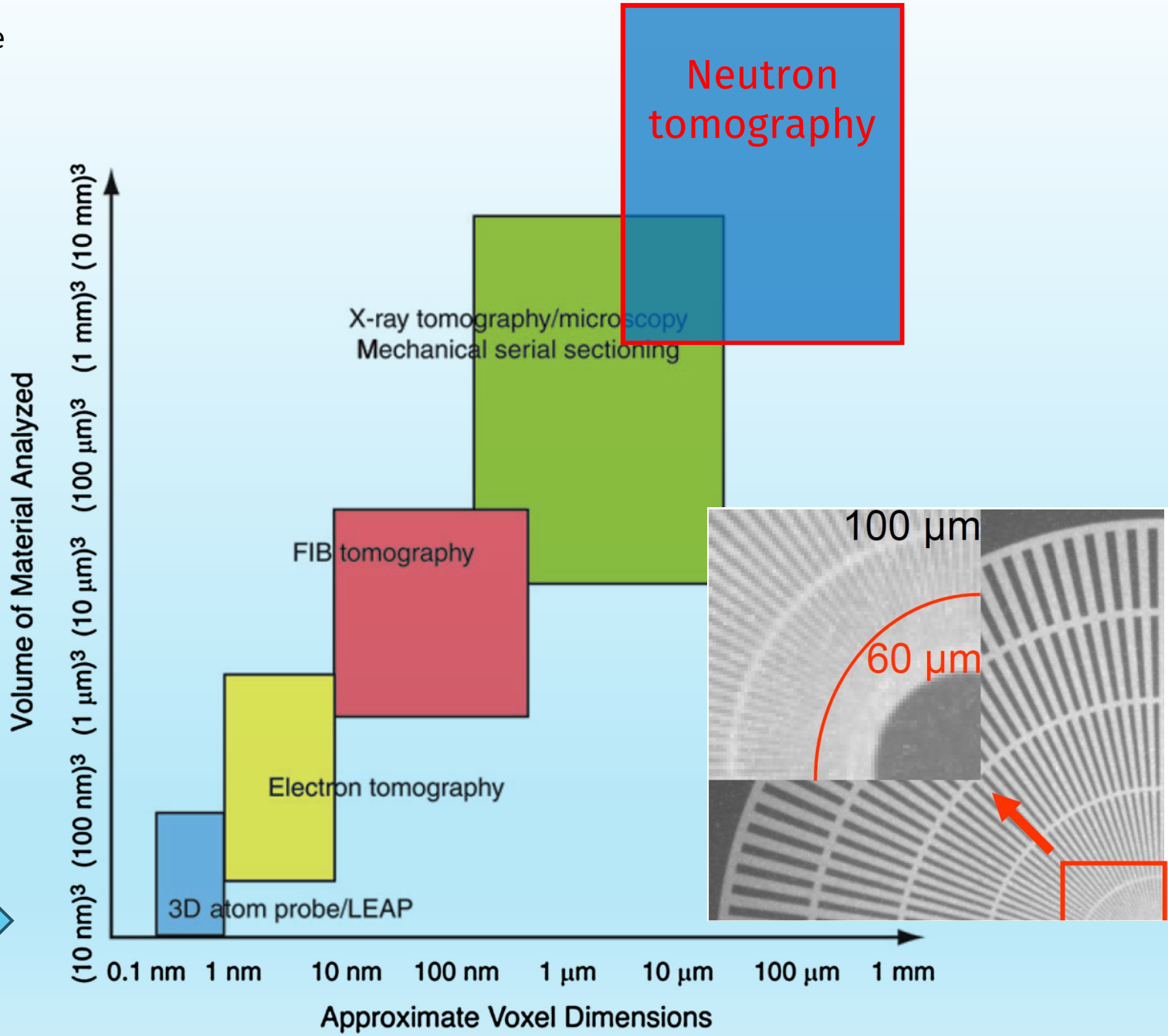

*S.N. Monteiro, S. Paciornik, JOM **69** No. 1 2017*

Neutron radiography and tomography

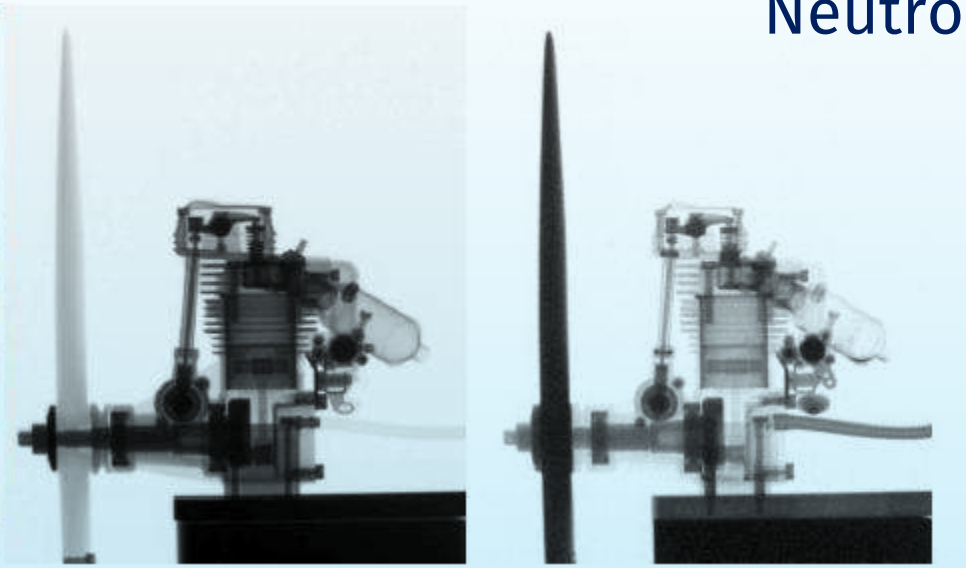

X-rays Neutrons

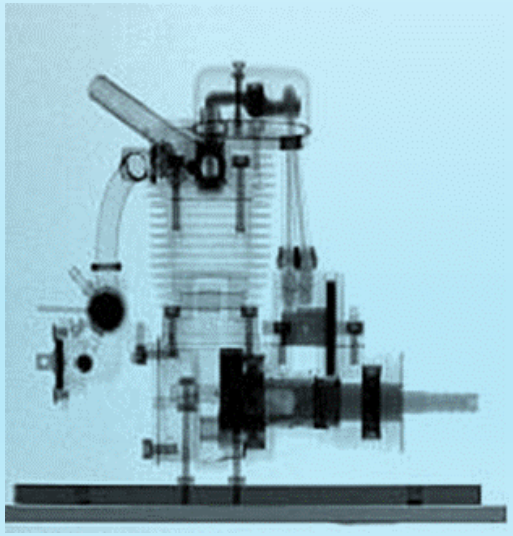

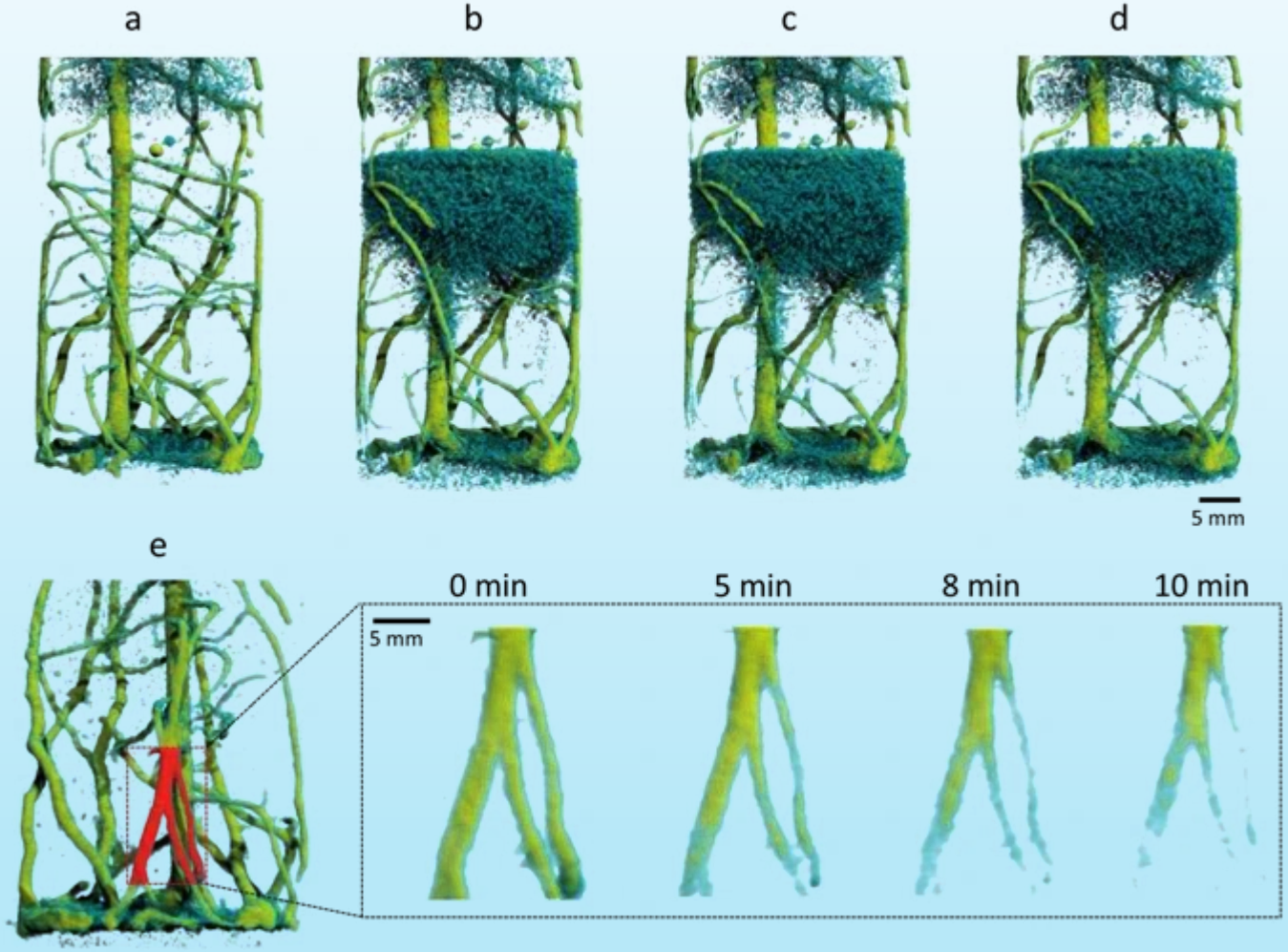

C. Tötzke, N. et al., Kardjilov, *Capturing 3D Water Flow in Rooted Soil by Ultra-fast Neutron Tomography*, Sci. Reports **7,** 6192

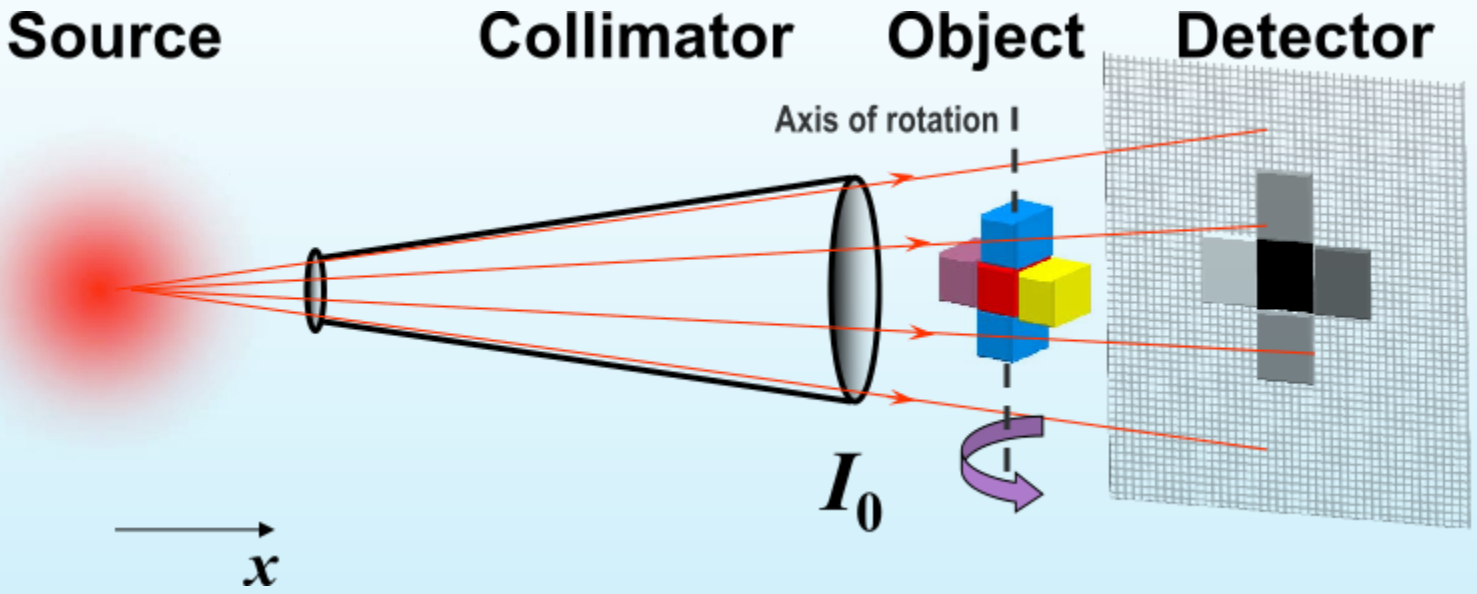

The Radon theorem (Johann Radon, 1917) and the „Fourier slice theorem" provide theoretical grounds for neutron tomography.

From single tomographic projections, we can reconstruct objects of interest.

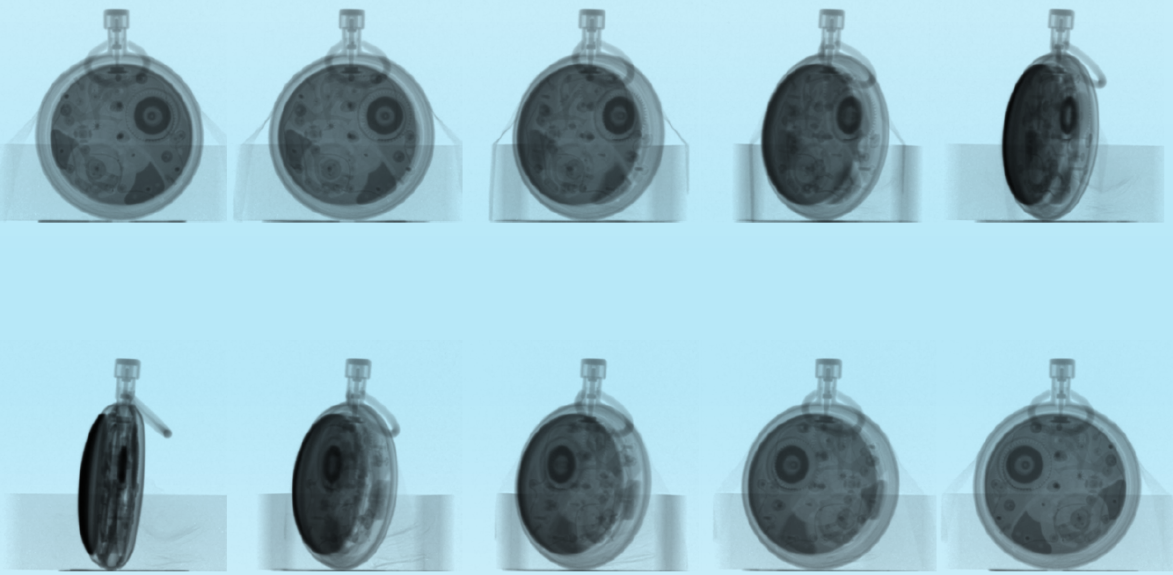

(N. Kardjilov, Oxford School on Neutron Scattering, 13. September 2017)

Scientific case:

Lithium cells cell in operando

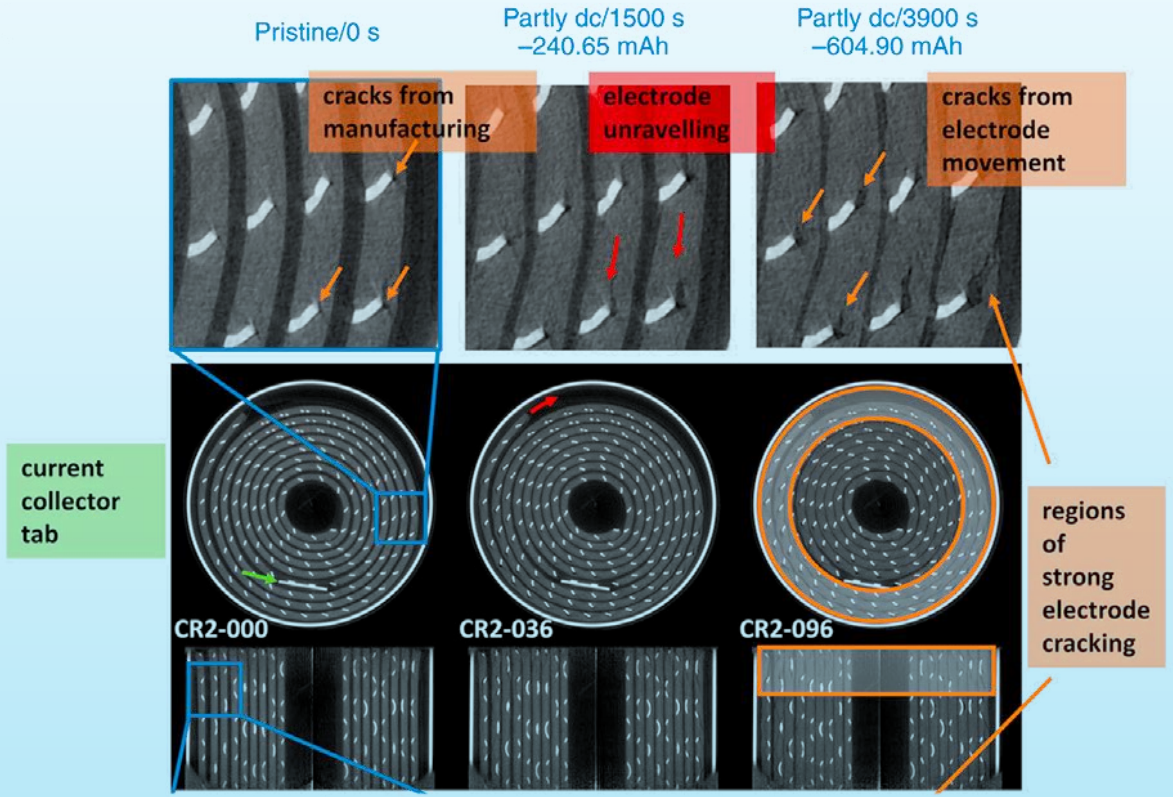

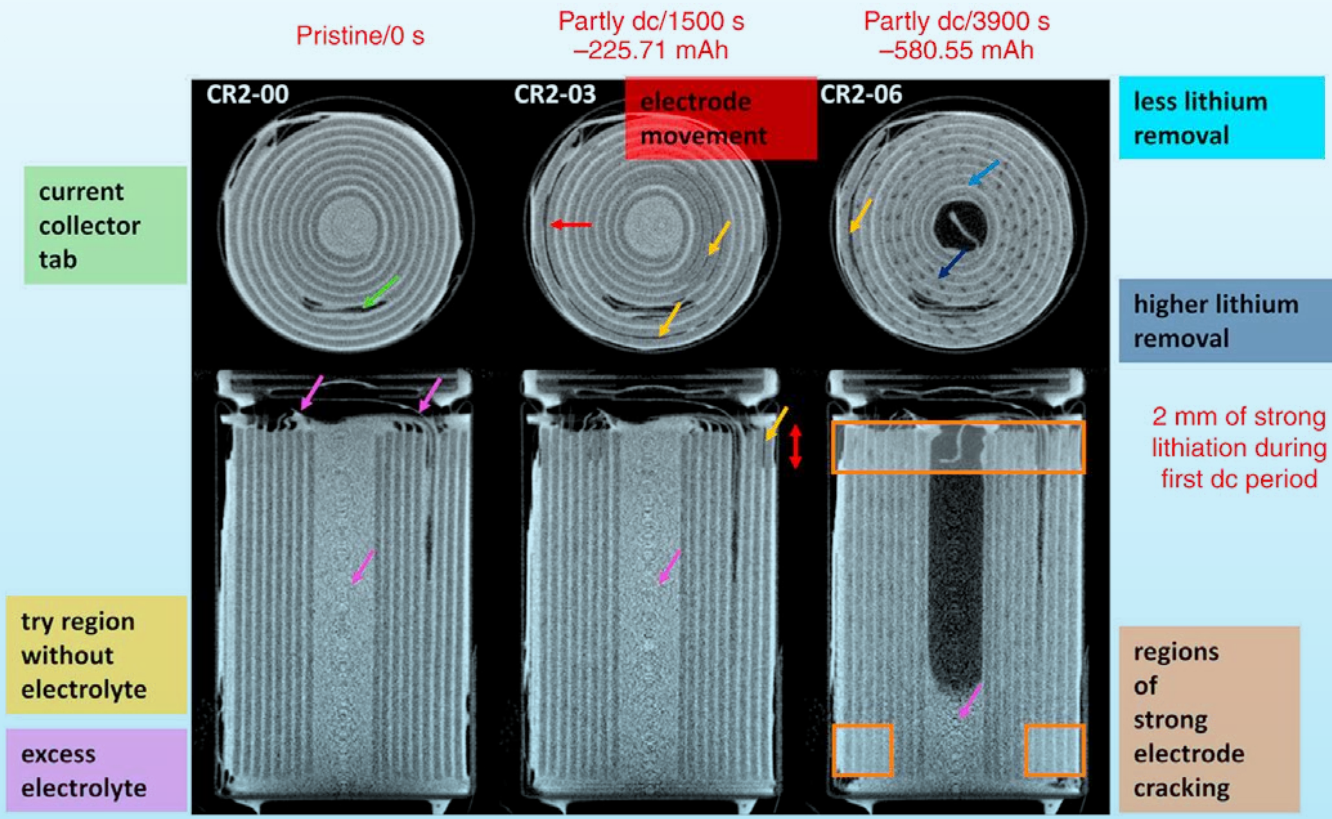

3D-reconstructed orthogonal slices of in operando X-ray CT (left) and N-CT (right) of a CR_2Li/MnO_2 cell during discharging over a 4.5 and a 4.7 Ω resistor.

X-ray (left) and neutron (middle) radiographs of a lithium-iodine cell after discharging, and rendered lithium distribution from an N-CT scan (right).

M. Strobl, I. Manke, et al., J. Phys. D: Applied Physics 42, 243001.

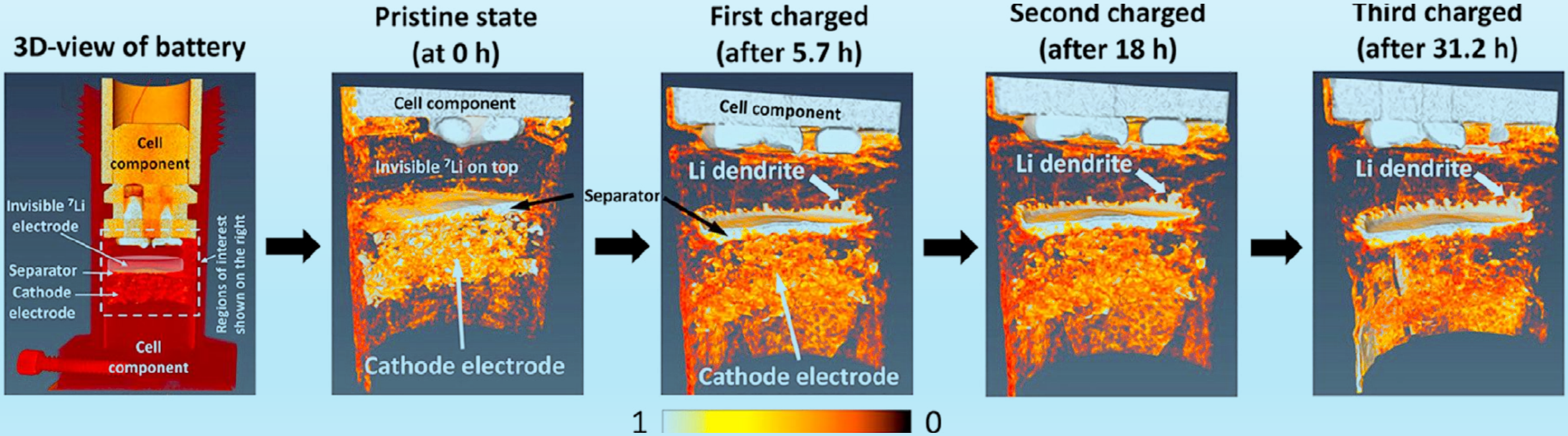

N-CT of dynamic dendrite growth in a $^7Li/LiMn_2O_4$ electrochemical half-cell at several stages of charge and the disappearance after discharge with a transparent ^{7}Li-anode.

B. Song, I. Dhiman, et al., ACS Energy Lett 4, 2402–2408, 2019

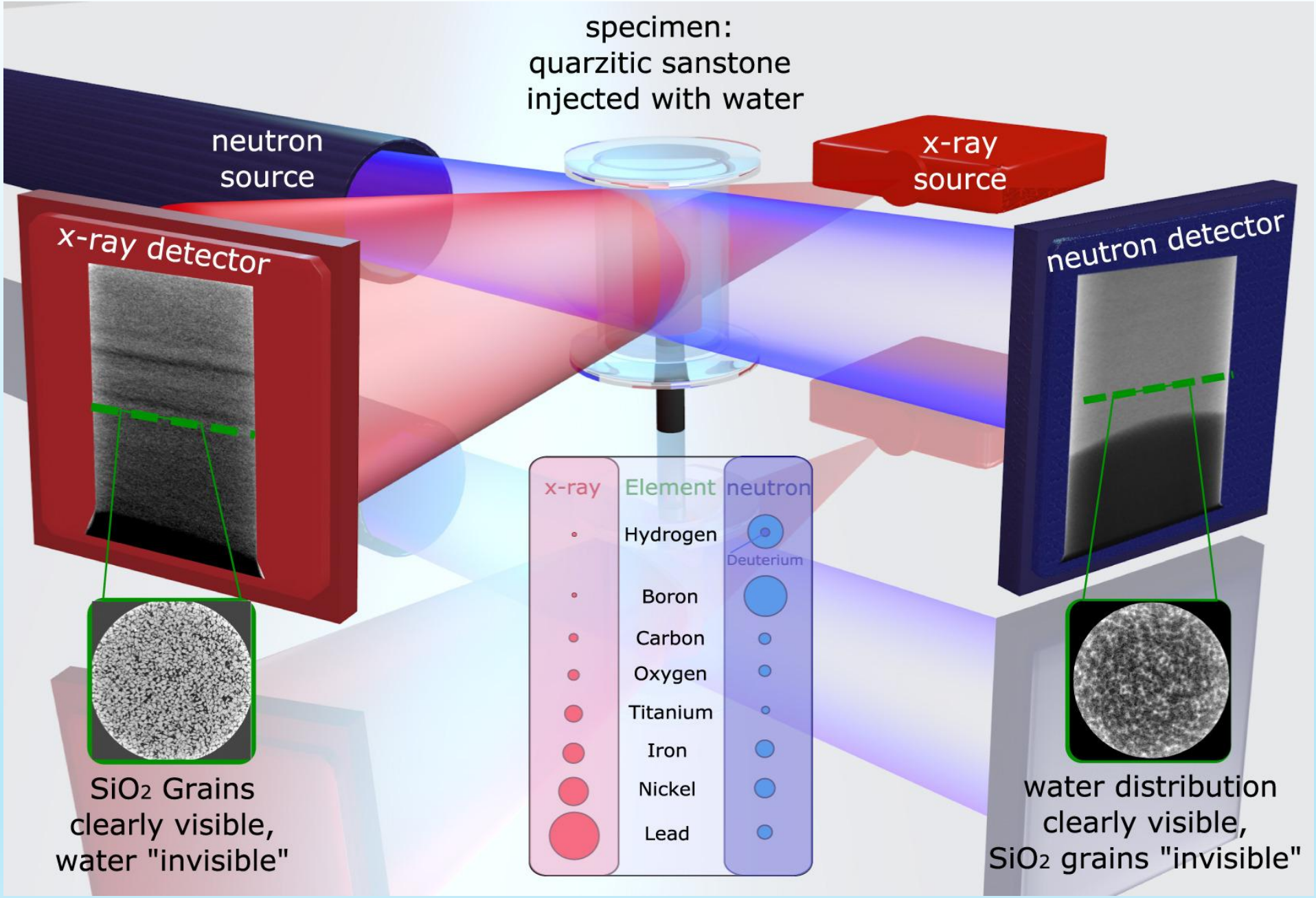

NeXT (Neutron and X-ray Tomograph)

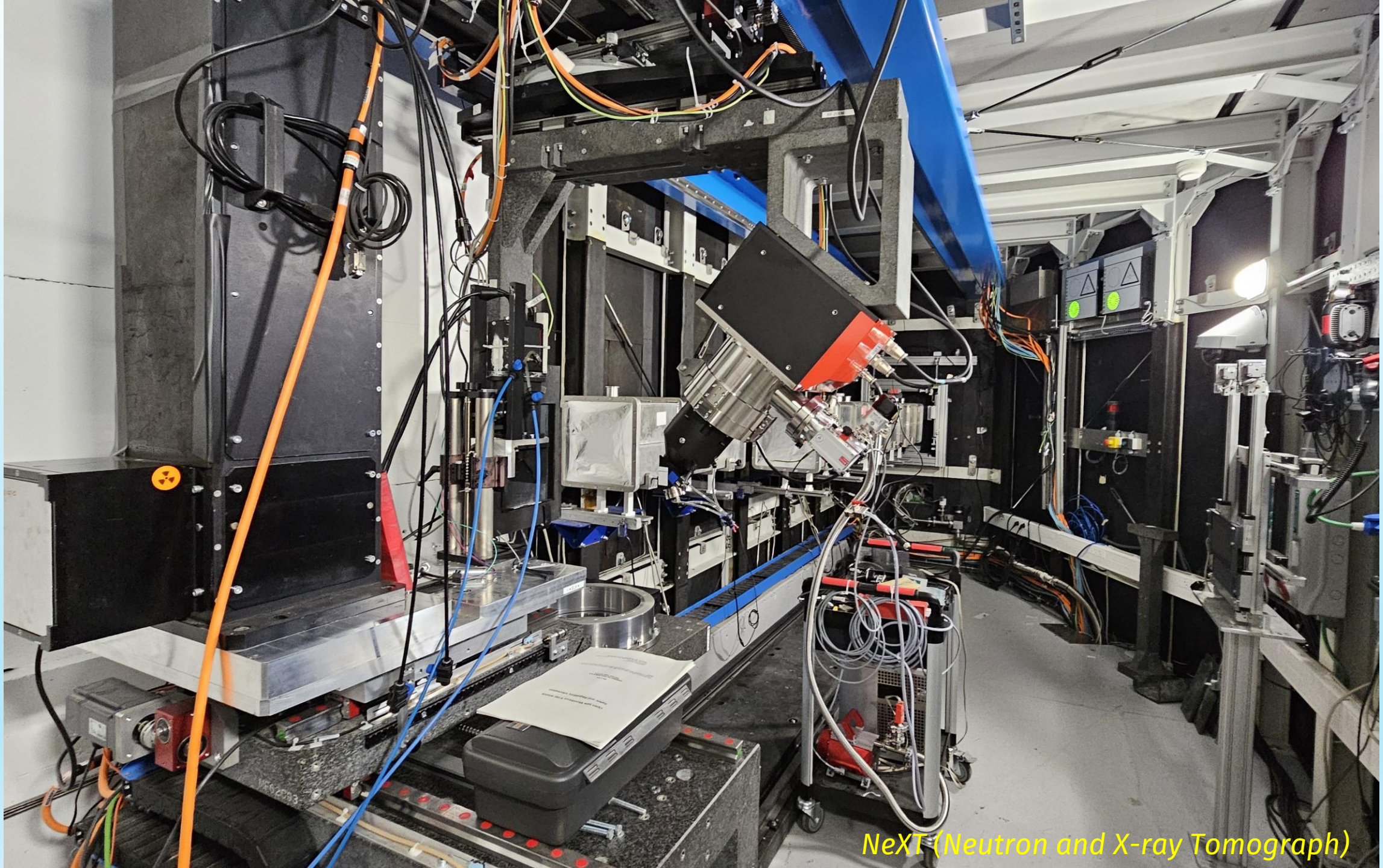

NeXT (Neutron and X-ray Tomograph)

Neutron scattering geometry

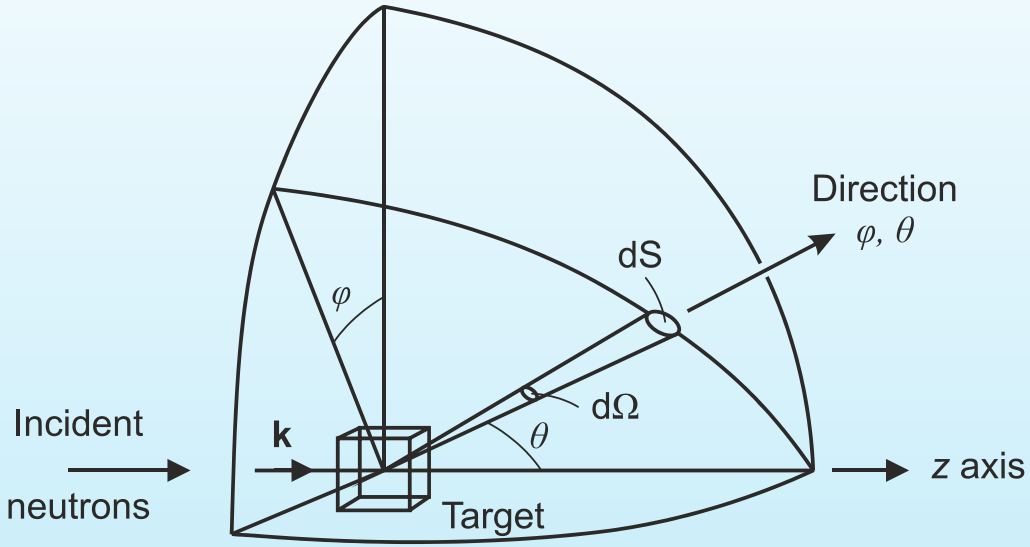

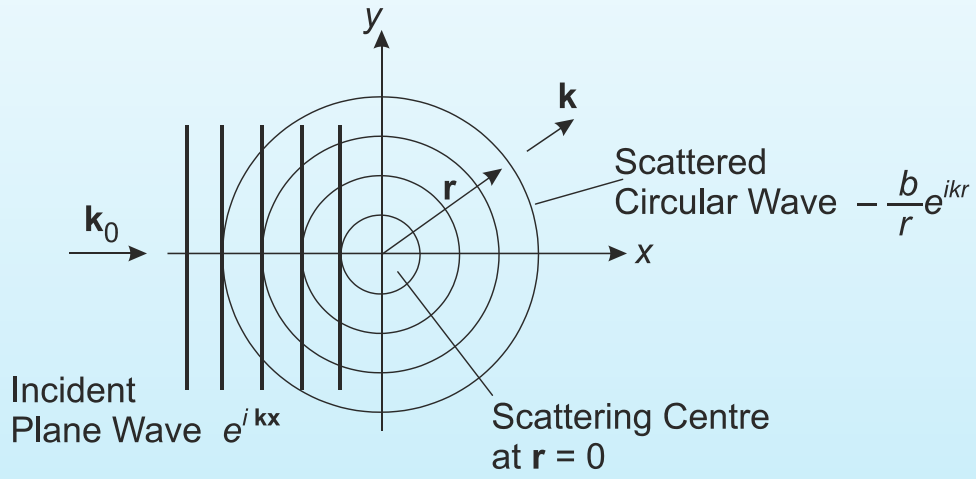

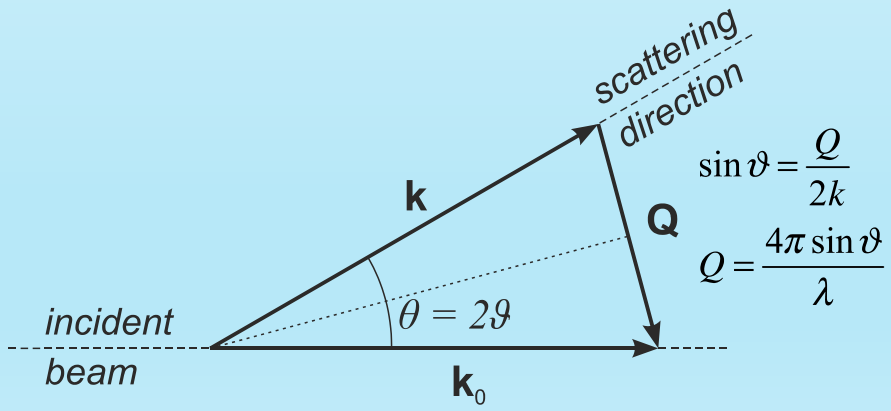

Elastic scattering

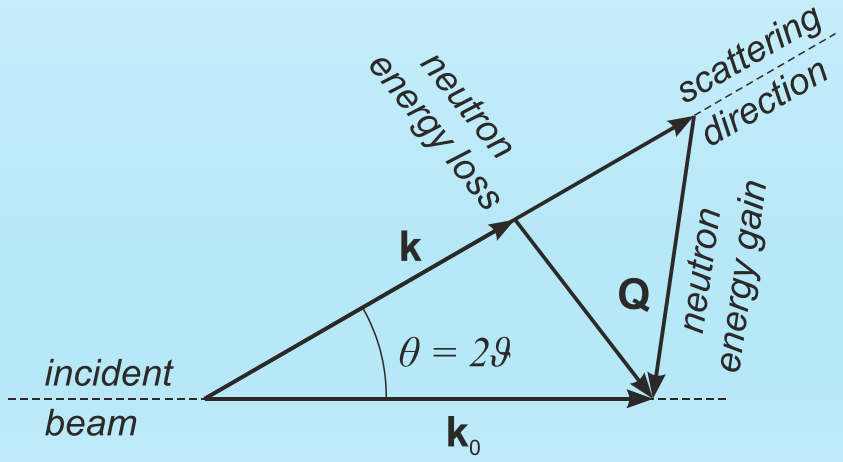

Inelastic scattering

The scattering cross section: a heuristic approach

The physical meaning of a cross section σ is a measure of the probability of a reaction.

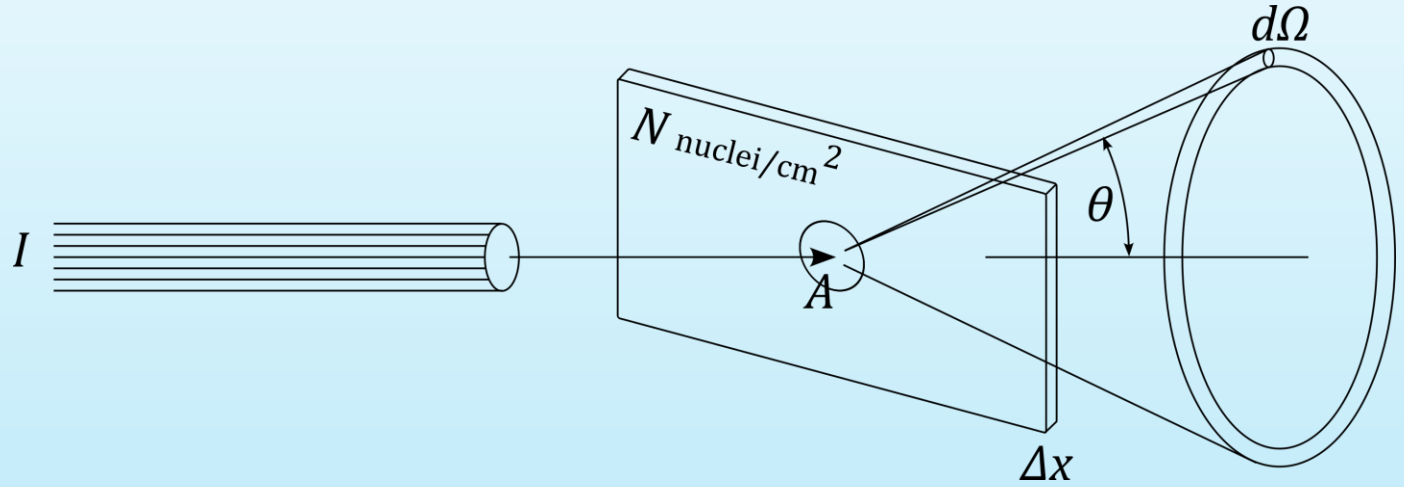

Schematic drawing of an incident beam striking a thin target with a particle emitted into a cone subtending an angle θ relative to the direction of incidence, the 'scattering' angle. The element of solid angle $d\Omega$ is a small piece of the cone.

The angular differential cross section $\frac{d\sigma}{d\Omega}$ can be seen as the number of reactions per second in an angular cone subtended at angle θ with respect to the direction of incidence.

cf. Sidney Yip, lecture 7 (10/2/06)

Laying the ground: a few simple formulae

Theoretical treatment of neutron scattering usually starts with the quantum mechanical description of a two-body collision.

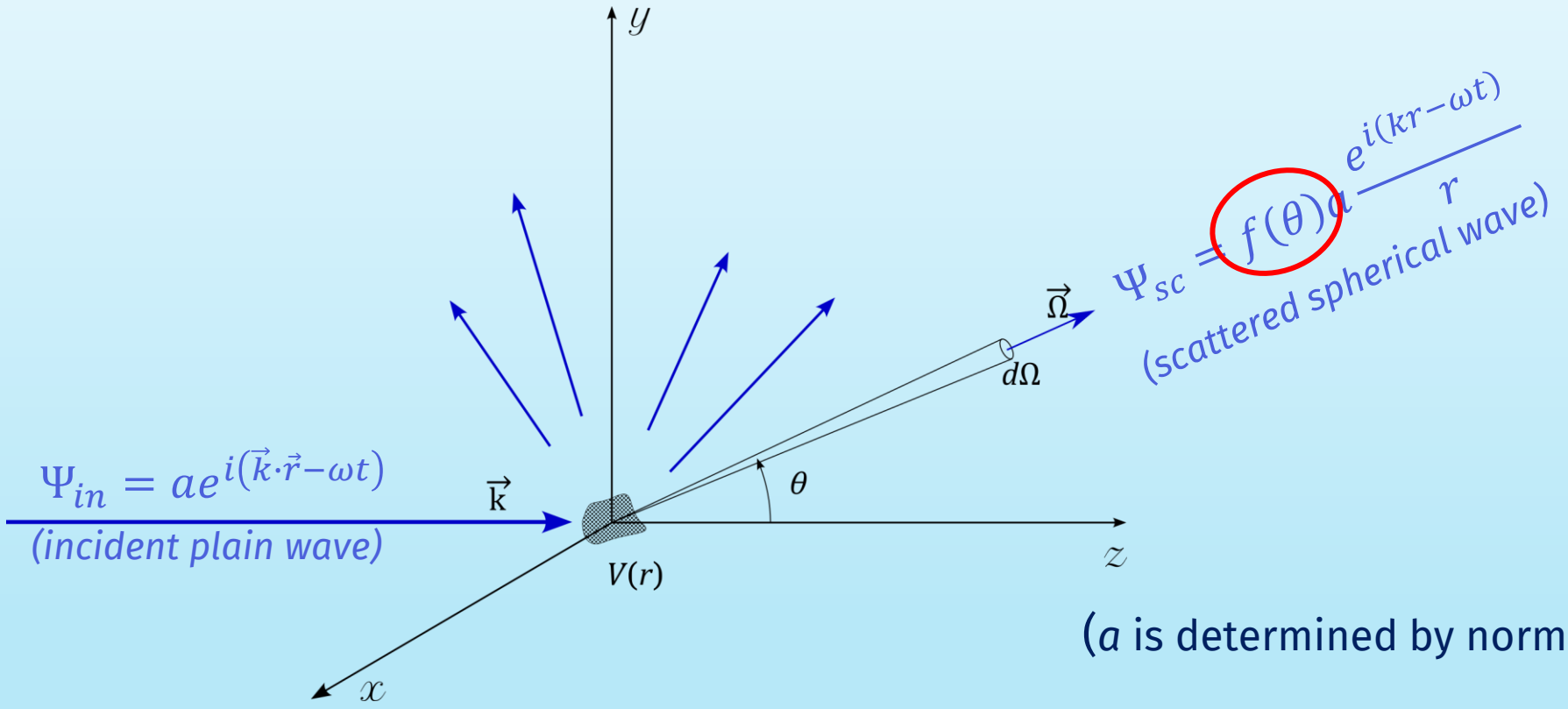

(*a* is determined by normalization condition.)

$f(\theta)$ denotes the amplitude of scattering in the direction of angle θ relative to the direction of incidence.

$$\frac{d\sigma(\theta)}{d\Omega} = |f(\theta)|^2$$

This is the fundamental expression relating the scattering amplitude to the cross section.

$$f(\theta) = -\frac{2\mu}{4\pi\hbar^2}\int d^3r\, e^{i\mathbf{Q}\cdot\mathbf{r}}\, V(\mathbf{r}) \qquad \mathbf{Q} = \mathbf{k}_0 - \mathbf{k}$$

In the Born approximation the scattering amplitude is given by the Fourier transform of the interaction potential. The Fourier transform variable **Q** is a wave vector, the difference between the wave vectors of the scattered and incident waves **k** and $\mathbf{k}_0$, **Q** is referred to as the ***wave vector transfer*** or the ***scattering vector***.

Elementary scattering theory

Strictly speaking, the validity conditio of the Born approximation with the "true" interaction potential is not fulfilled in the case of thermal neutron scattering. This was first noticed and solved by E. Fermi. He introduced a pseudopotential in place of the actual neutron-nucleus interaction by distorting the latter through extending the range and decreasing the depth so that the transformation preserves the scattering length.

The fictitious Fermi potential $V^*(r)$, or pseudopotential, has the well depth and range scaled so that $V^*(r)$ is a spherical well with depth V_0^* and range r_0^*.

$$V^*(r) = \frac{2\pi\hbar^2}{m} b\delta(r)$$

b, being in general a complex nuber $b = b' + ib''$, is known as the bound **scattering length**, "bound" because it refers to the fixed nucleus.

This formula has an important advantage: the correct scattering cross section is already built into the potential.

In the low-energy limit the scattering (s-wave) cross section and the absorption cross section far form resonant capture are given by:

$$\sigma_s = 4\pi|b|^2 \qquad \sigma_a = \frac{4\pi}{k_0} b''$$

Where do the coherent and incoherent σ's and b's come from?

Still within the Born approximation: If the target nucleus has a non-zero spin then the neutron and nuclear spins could be either parallel or antiparallel during the scattering process. The neutron, being a fermion with spin ½, couples to the nuclear spin I to give :

Spin operators	Eigenvalues	Number of degenerate states	Relative weights
$\vec{I}+\frac{\vec{1}}{2}$	$I+{}^1/_2$	$2(I+{}^1/_2)+1=2I+2$	$W_+=\frac{2I+2}{4I+2}=\frac{I+1}{2I+1}$
	$I-{}^1/_2$	$2(I-{}^1/_2)+1=2I$	$W_-=\frac{2I}{4I+2}=\frac{I}{2I+1}$

- $2(I+1)$ degenerate states for the eigenvalue of $I+\frac{1}{2}$, corresponding to parallel arrangement of the neutron and nucleus spins, with the scattering length conventionally denoted by b_+.
- $2I$ degenerate states for the eigenvalue of $I-\frac{1}{2}$, corresponding to antiparallel arrangement of both spins. The related scattering length is denoted by b_-.

There are therefore altogether $2(2I+1)$ states with relative weights W_+ and W_- (Breit-Wigner formalism).

Averaging over spins: $\bar{b} = W_+ b_+ + W_- b_- = \frac{(I+1)b_+ + I b_-}{2I+1}$ $\quad \overline{b^2} = W_+ b_+^2 + W_- b_-^2 = \frac{(I+1)b_+^2 + I b_-^2}{2I+1}$

Coherent scattering length: $b_{coh} = \bar{b} = W_+ b_+ + W_- b_-$ ← Average

Incoherent scattering length: $b_{inc} = \sqrt{\overline{b^2} - \bar{b}^2} = \sqrt{W_+ W_-}(b_- - b_+)$ ← SQRT(variance)

Coherent scattering length is the weighted average of b_+ and b_- , while incoherent scattering length is given by the variance of b_+ and b_-:

Zero-spin nuclei have $b_{inc} = 0$, hence in an experiment they show no incoherent scattering
(other sources of incoherence are still possible).

The corresponding cross sections are: $\sigma_{coh} = 4\pi b_{coh}^2$ $\quad \sigma_{inc} = 4\pi b_{inc}^2$

Coherent scattering is Q-dependent and therefore it carries structural information.

'wrap-up' #1: Coherent and spin-incoherent scattering

Coherent scattering

Incoherent scattering

Elastic

Inelastic

Elastic

Inelastic

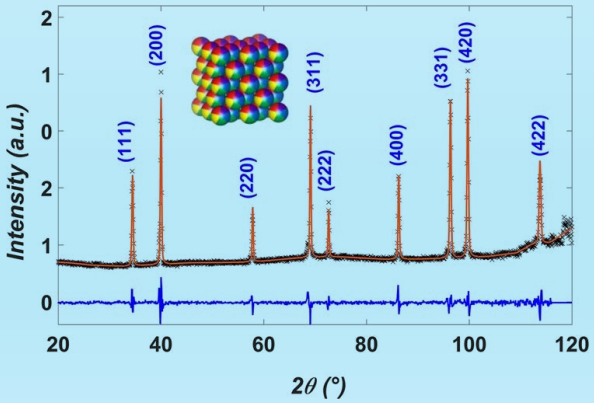

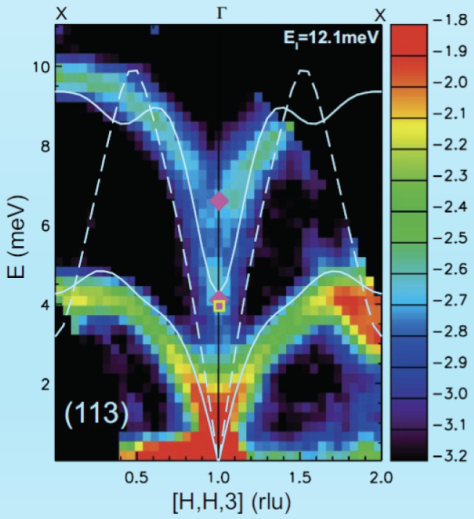

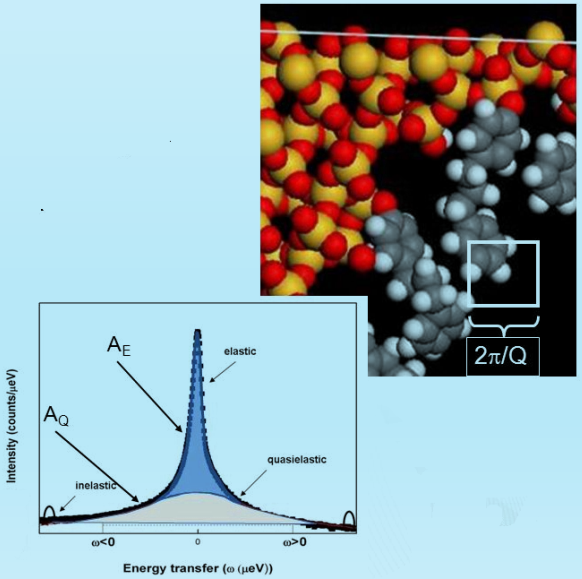

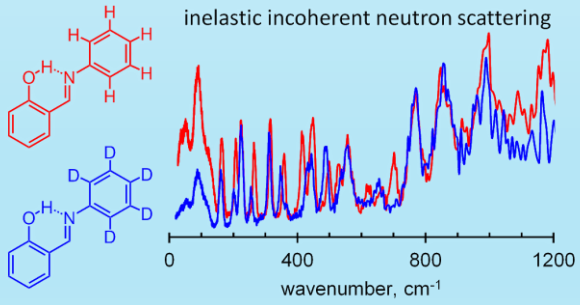

Neutron magnetic scattering scattering

The neutron possesses an inherent magnetic moment related to its spin-angular momentum.

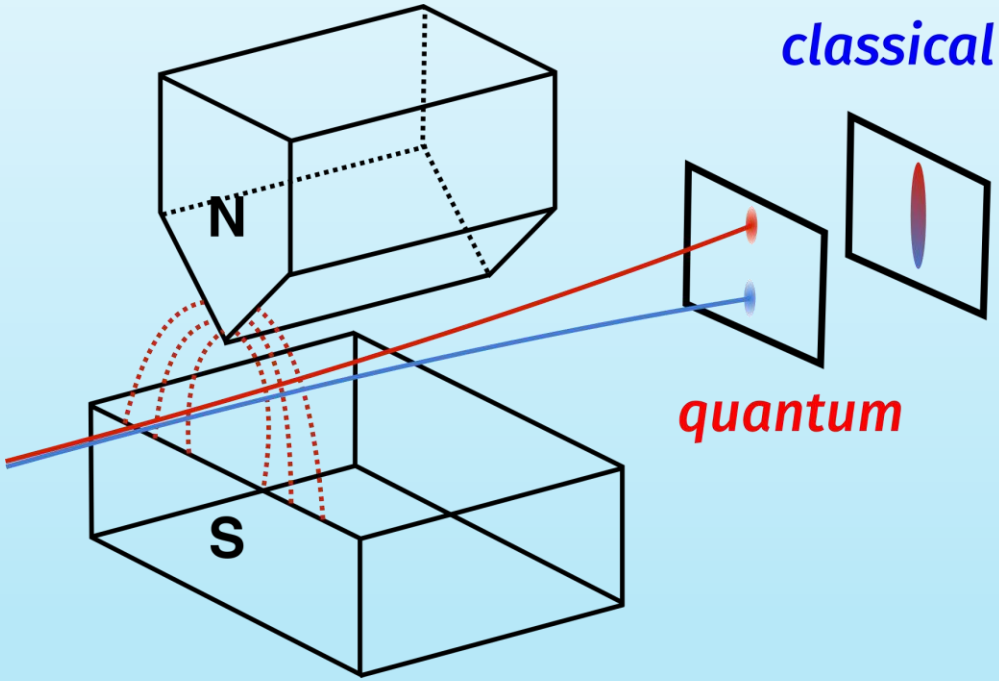

Stern, Gerlach (1922)

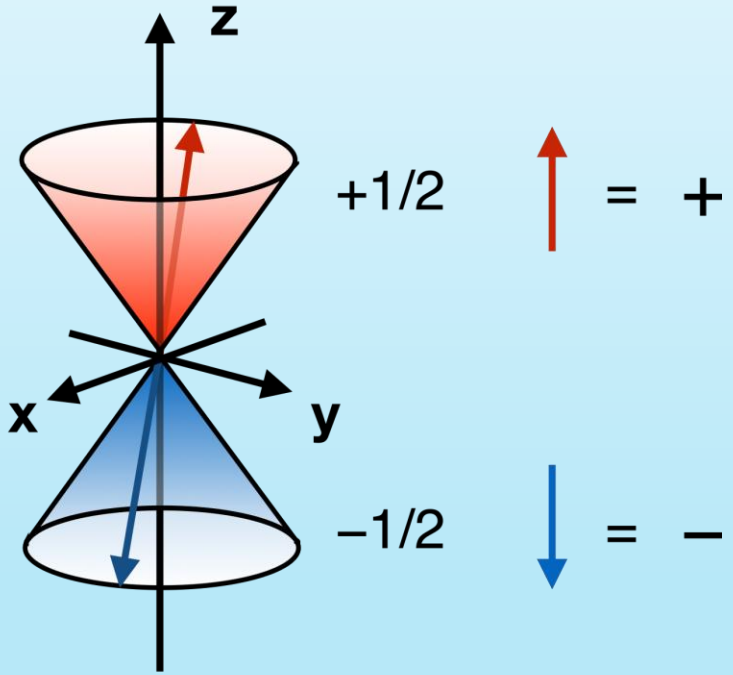

Spin and magnetic moment are oppositely oriented, complicating what "up" and "down" mean with respect to an applied field.

Let s_i, s_f and ℓ_i, ℓ_f be the initial and final states of the neutron and of the scattering system, respectively. Then, in the Born approximation the scattering cross section contains this matrix element:

$$\langle s_f \ell_f \,|\, V(\mathbf{Q}) \,|\, s_i \ell_i \rangle$$

where $V(\mathbf{Q})$ is the Fourier transform of the interaction potential $V(\mathbf{r})$:

$$V(\mathbf{Q}) = \int V(\mathbf{r})\; e^{i\mathbf{R}\cdot\mathbf{r}}\; d^3r$$

In general, the potential $V(\mathbf{Q})$ can be written as a sum of spin-inependent and vector-type terms:

$$V(\mathbf{Q}) = \frac{2\pi\hbar}{m_n}\left[V_{si}(\mathbf{Q}) + V_v(\mathbf{Q})\right]$$

For convenience, both components are sometimes represented in this way:

	$V_{si}(\mathbf{Q})$	$V_v(\mathbf{Q})$
Nuclear	$\sum_j A_j \exp(i\mathbf{Q}\cdot\mathbf{r}_j)$	$\frac{1}{2}\sum_j B_j \mathbf{I}_j \exp(i\mathbf{Q}\cdot\mathbf{r}_j)$
Magnetic	0	$\frac{\gamma r_0}{2\mu_B}\mathbf{M}_\perp(\mathbf{Q})$
Electric*)	$\frac{\gamma r_0}{2}\frac{m_e}{m_n}n(\mathbf{Q})$	$\frac{\gamma r_0}{2}\frac{m_e}{m_n}n(\mathbf{Q})i\cot\left(\frac{\phi}{2}\right)\hat{\mathbf{z}}$

*) Electric interactions:

- spin-orbit coupling
- Foldy interaction due to the existence of internal electric fields within the neutron

'wrap-up' #2: The neutron as a measuring probe

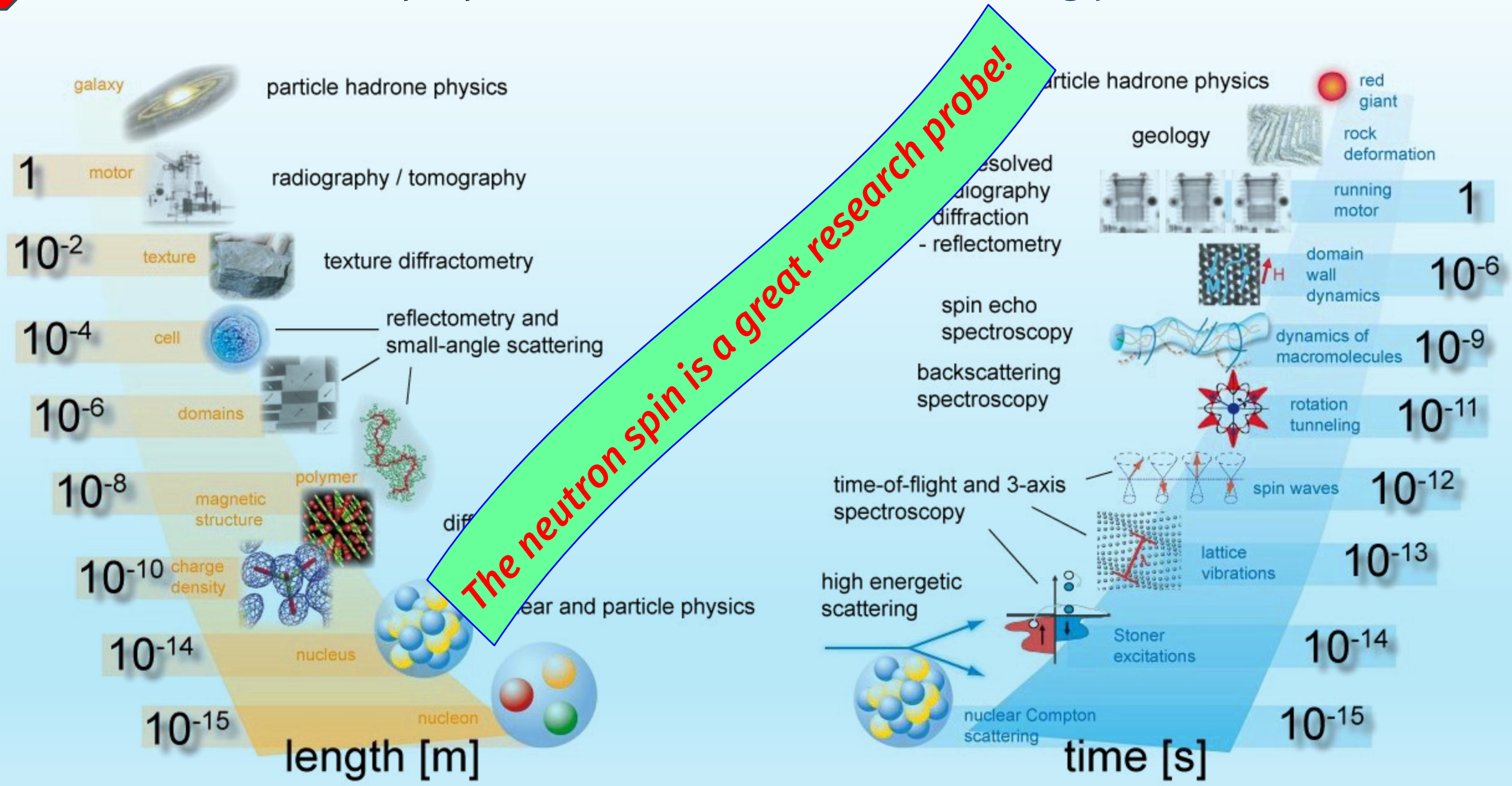

Examples: neutron diffraction

Scientific case: High Entropy and multicomponent alloys

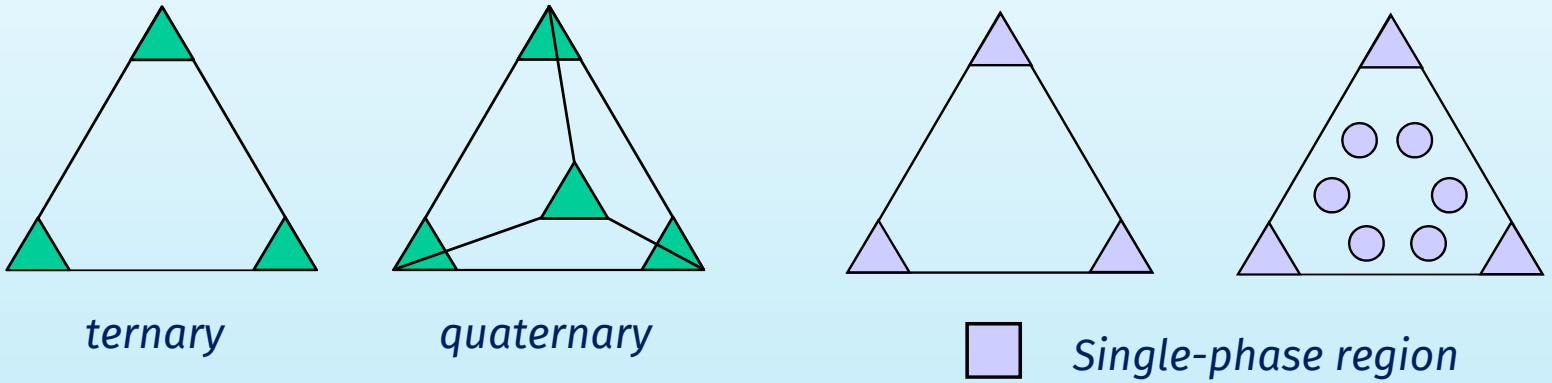

Schematic ternary and quaternary systems, showing regions of the phase diagram which are relatively well known near the corners, and relatively less well known near the centre.

Solution vs. compound:

$A + B = AB_{solution}$: $\Delta G_{mix} = \Delta G_{mix} - T\Delta S_{mix}$

$A + B = AB_{intermetallic}$: $\Delta G_f = \Delta G_f - T\Delta S_f$

In alloys with a high number of principal elements (say, $n = 5$), the entropic contribution to the free energy ($-T_m\Delta S_{mix}$) at the melting temperature T_m is comparable to the formation enthalpies (ΔH_f) of strong intermetallic compounds such as NiAl and TiAl, thereby suppressing compound formation, except those with large heats of formation, such as strong ceramic compounds (oxides, carbides, nitrides and silicides), and more easily yielding random solid solutions during solidification.

High Entropy and magnetic alloys

Property	Projected Trend (HEA vs conventional)	Rationale for Projection
Saturation Magnetization (M_s)	Lower	Lower content of ferromagnetic elements
Intrinsic Coercivity ($_iH_c$)	Higher	Lattice structures will tend to pin domain walls
Permeability (μ)	Lower	Lower content of high permeability elements
Electrical Resistivity	Higher	Greater lattice distortion; potentially higher content of non-metallic elements
Curie Temperature (T_c)	May be higher or lower	Less compact lattices tend to reduce T_c; smaller particle sizes tend to reduce T_c; changes in crystal structure and in alloying elements can raise or lower T_c.
Corrosion Resistance	Higher	Cocktail effect promotes the formation of various surface oxide films.
Wear Resistance	Higher	Severe lattice distortion tend to improve hardness and strength, high temperature softening resistance tend to facilitate high wear resistance.

For HEAs, the central questions are:

- how coherent wave propagation is possible amidst structural disorder,
- how magnetic order stabilises the crystal structure.

Determining the direction of magnetic moments for CrMnFeCoNi HEA with the aid of preferred orientation due to tensile loading.

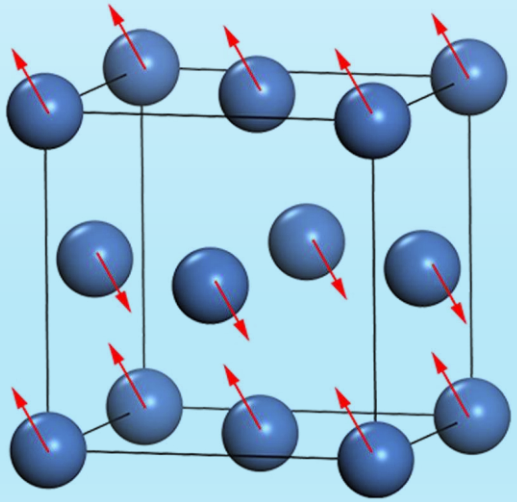

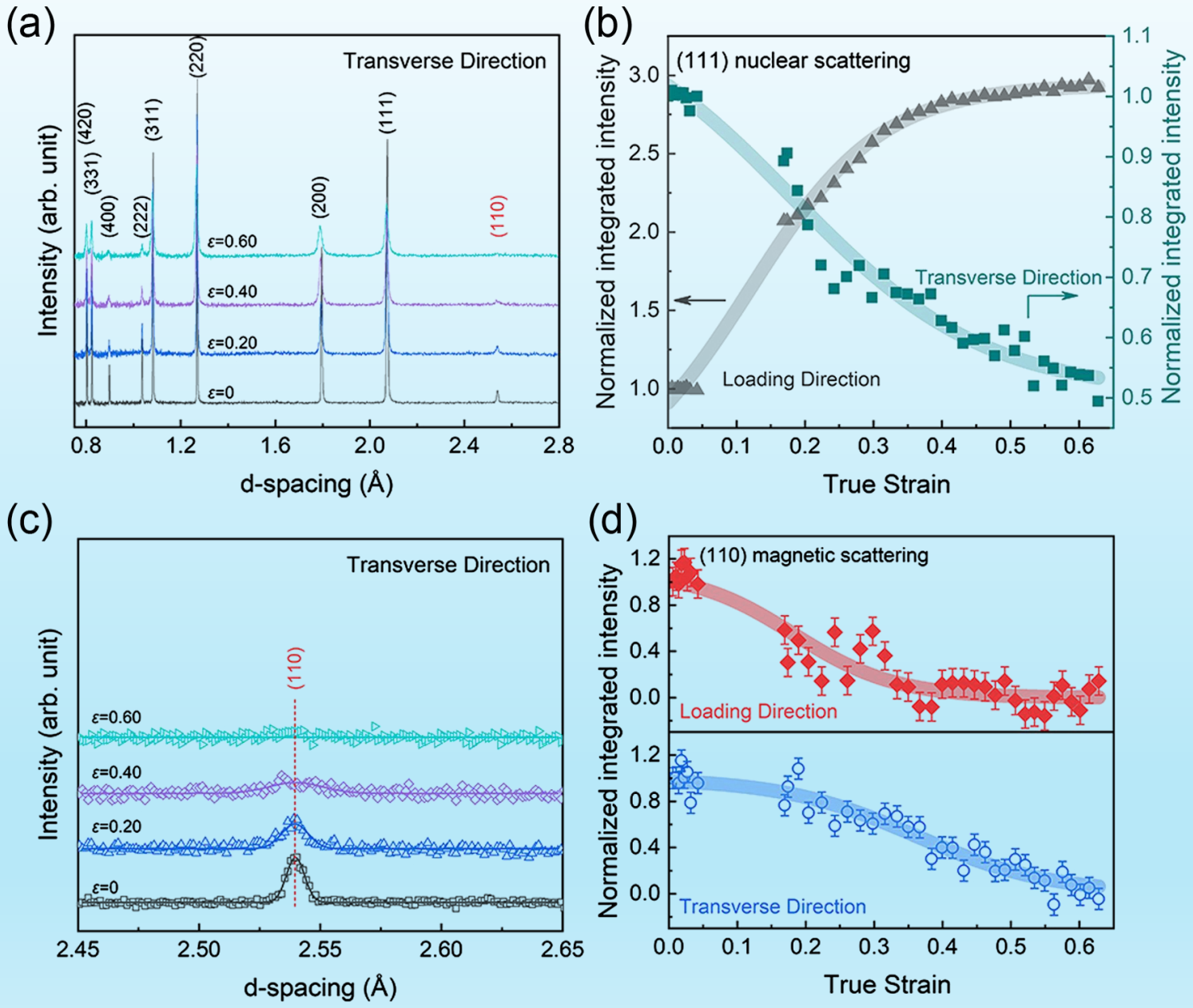

L. Zhu, H. He, M. Naeem et al., Phys. Rev. Lett. ***133*** *126701 (2024)*

Scientific case:

Metal-Organic Frameworks (MOFs)

Magnetocaloric effect in low applied magnetic fields in $LnOHCO_3$ (Ln = Gd^{3+}, Tb^{3+}, Dy^{3+}, Ho^{3+}, and Er^{3+}) frameworks.

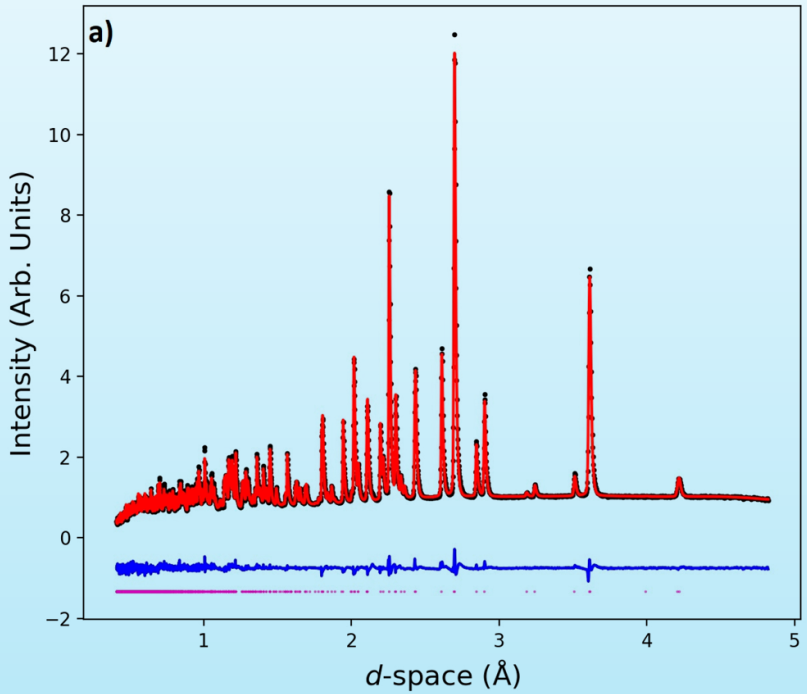

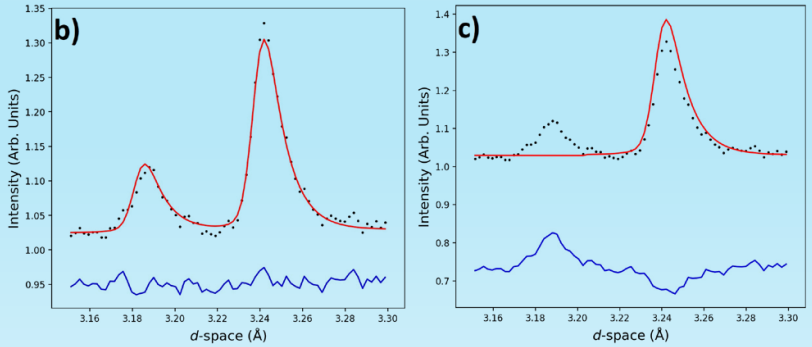

Neutron diffraction patterns of $TbODCO_3$ at 100 K from banks 5 and 6 of the WISH diffractometer. (a) Rietveld fit in $P2_12_12_1$ space group, (b) close up of the (102) reflection at 3.18 Å, and correct fitting using $P2_12_12_1$ space group.

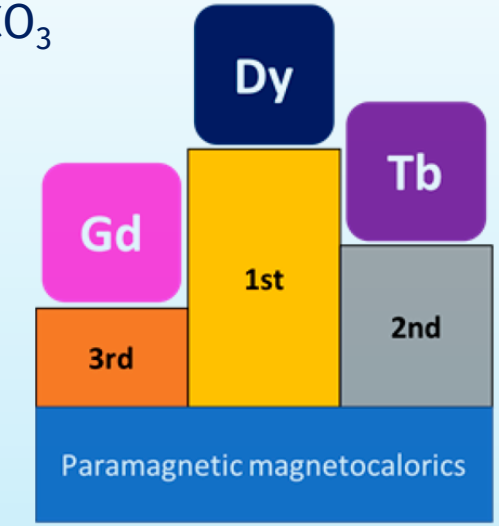

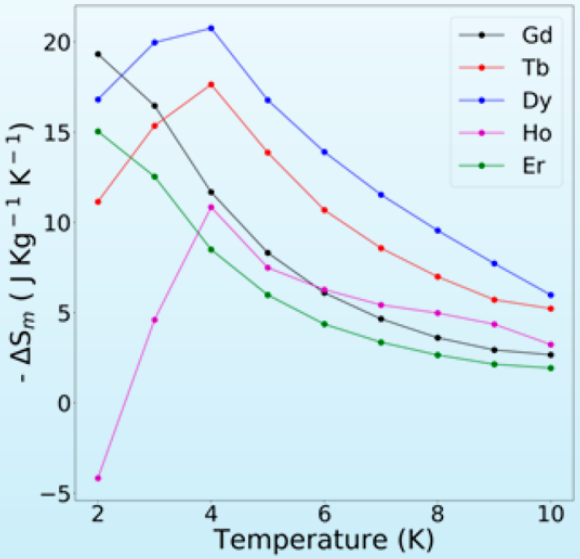

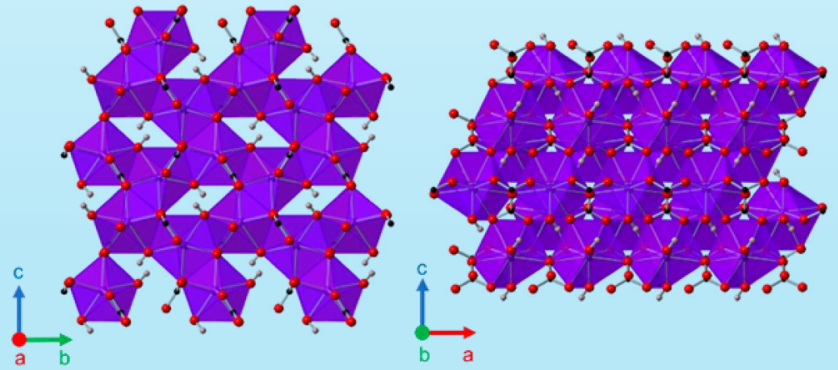

Polyhedral models of $LnOHCO_3$ in $P2_12_12_1$.

R.J.C Dixey, P.J. Saines, Inorg. Chem. ***57****, 12543–12551 (2018)*

Examples: neutron spectroscopy (INS)

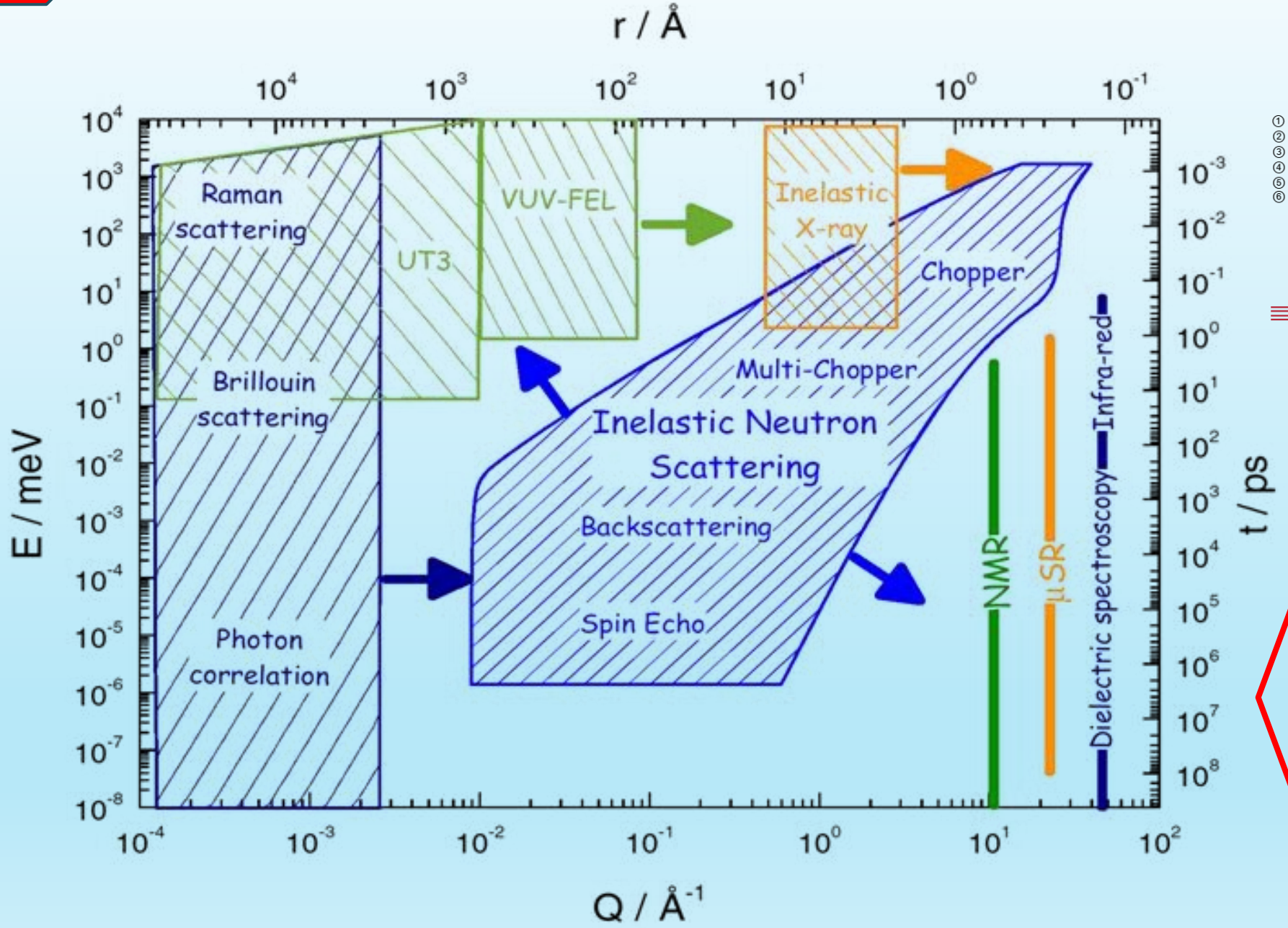

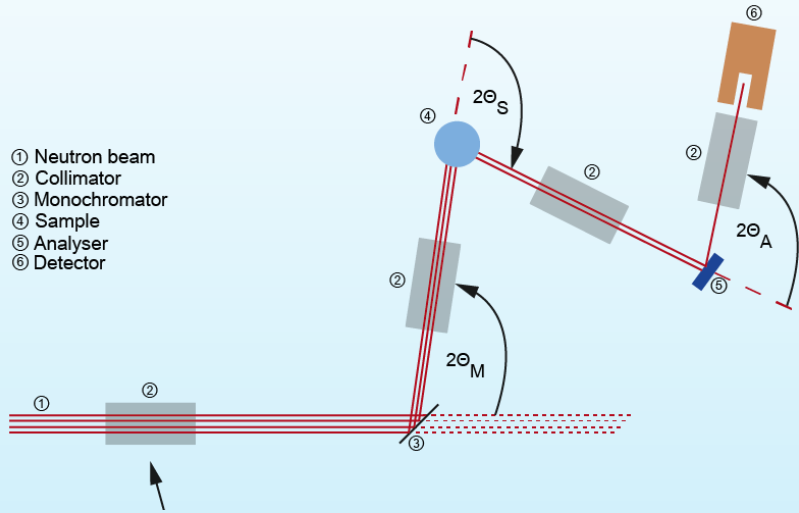

Dynamic ranges accessible by neutron spectroscopy related to other spectroscopic techniques nowadays available.

Neutron spectroscopy

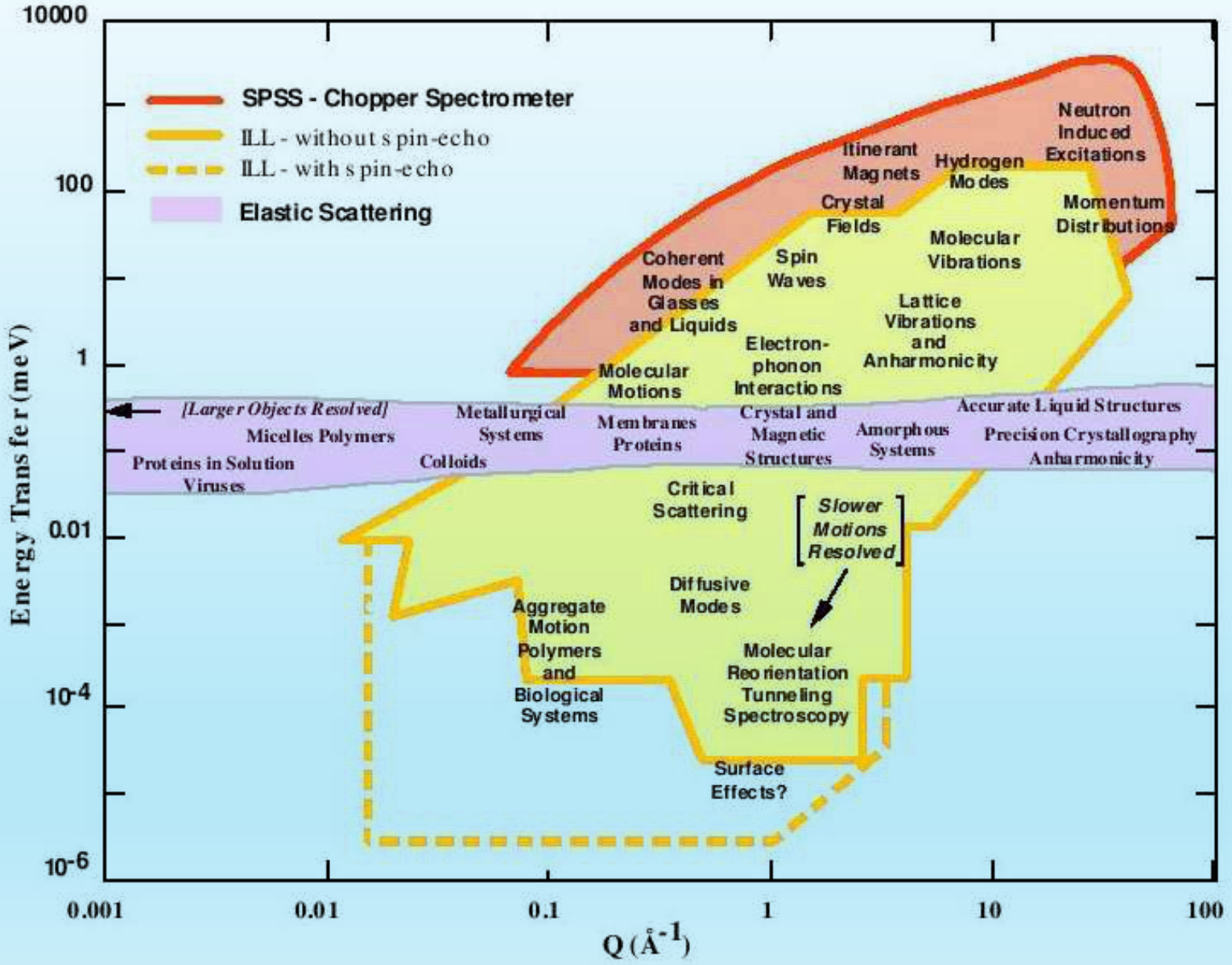

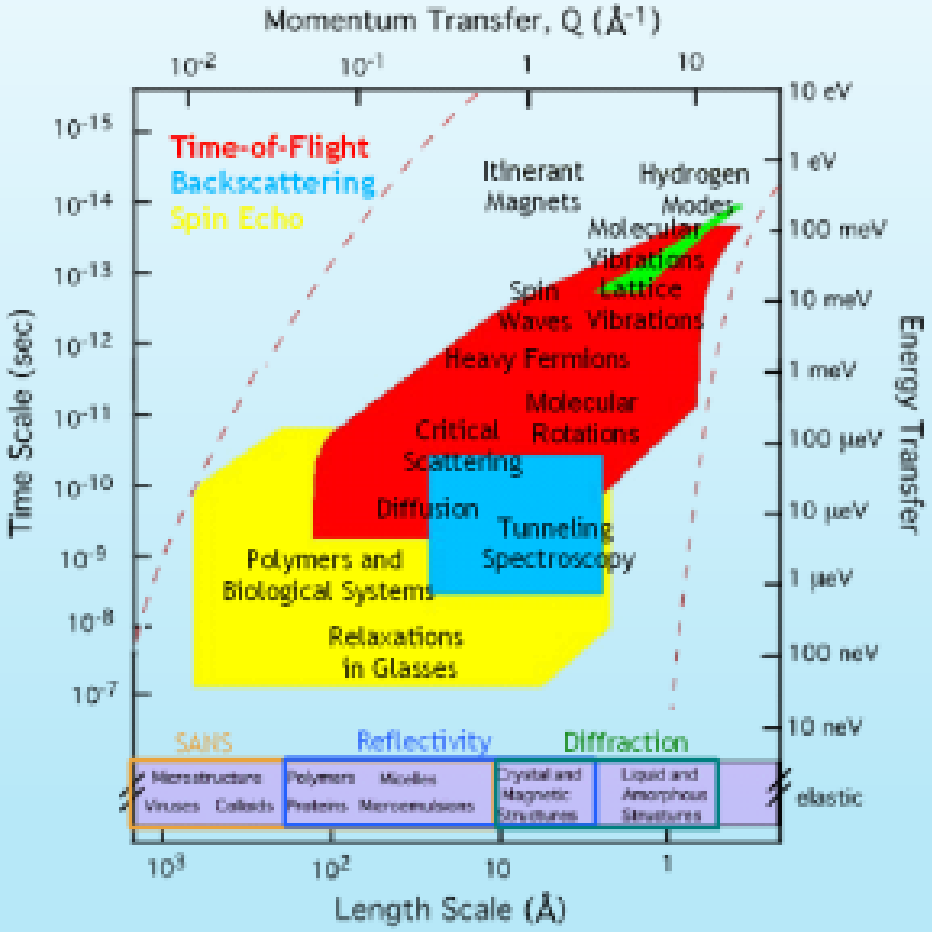

Scientific case (continued):

High Entropy and magnetic alloys

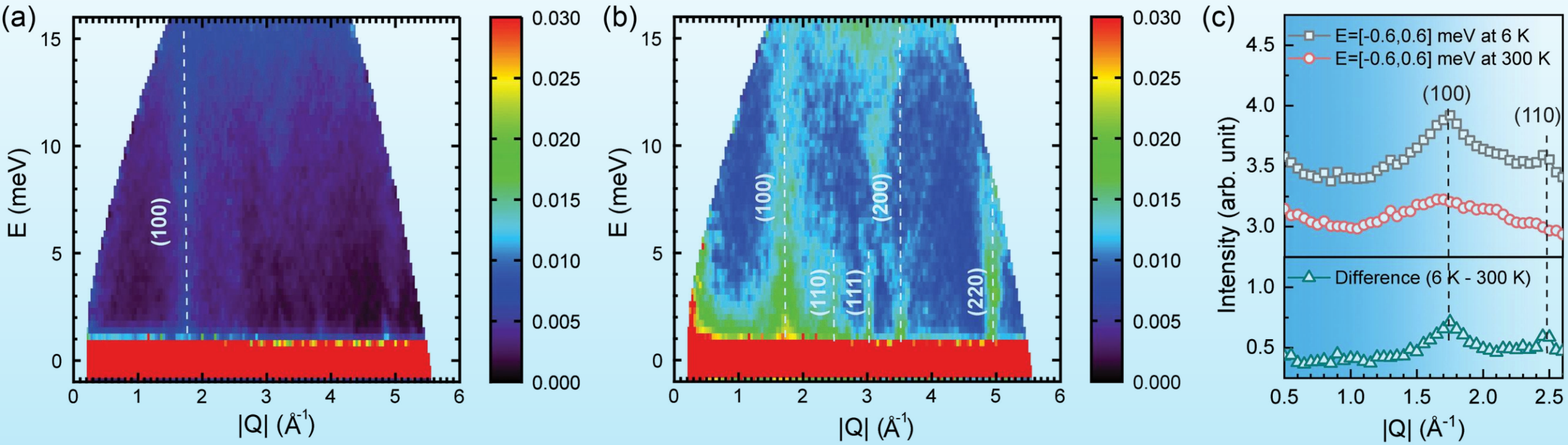

Spin dynamics in CrMnFeCoNi HEA determined by inelastic neutron scattering. Colour maps of the dynamic structure factor $S(Q,E)$ as functions of momentum transfer Q and energy transfer E at (a) 6 K and (b) 300 K. (c) Integrated dynamic structure factor $S(Q,E)$ over an energy transfer of $[-0.6;\ 0.6]$ meV to obtain the elastic scattering profile for the CrMnFeCoNi HEA at 6 K and 300 K.

L. Zhu, H. He, M. Naeem et al., Phys. Rev. Lett. ***133*** *126701 (2024)*

Scientific case:

$BiFeO_3$ is one of the most celebrated multiferroic materials and has highly desirable properties. It is the only known room-temperature multiferroic with $T_C \approx 1100$ K and $T_N \approx 650$ K, and exhibits one of the largest spontaneous electric polarisations, $P \approx 80\ \mu C\ cm^{-2}$.

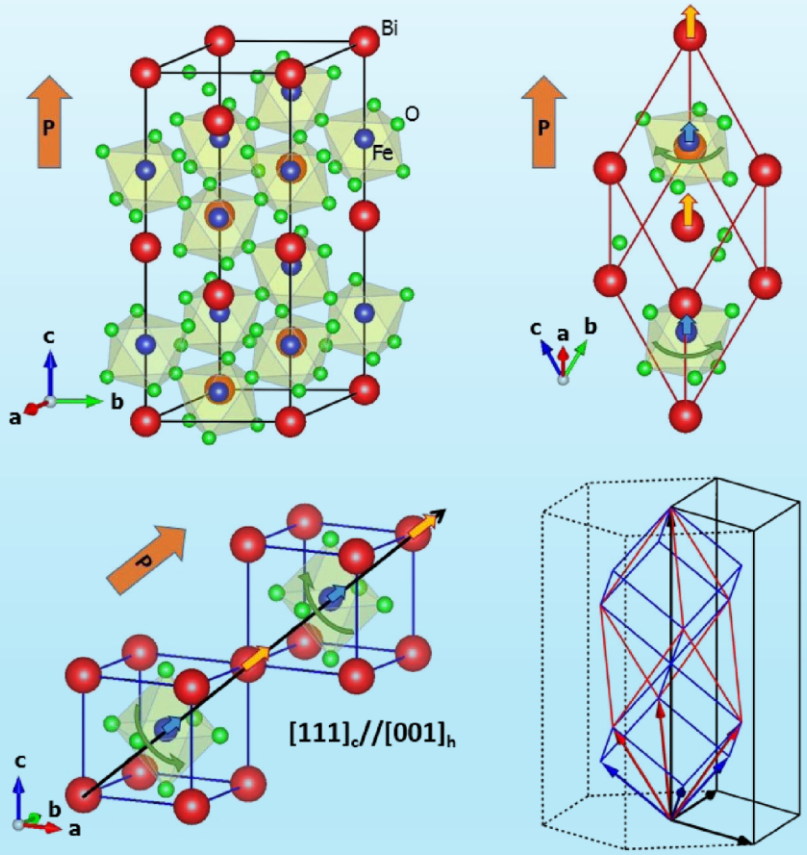

$BiFeO_3$ has a magnetic cycloid structure with an extremely long period of 620 Å, which arises from competition between the usual symmetric exchange interaction and the antisymmetric Dzyaloshinskii–Moriya (DM) interaction.

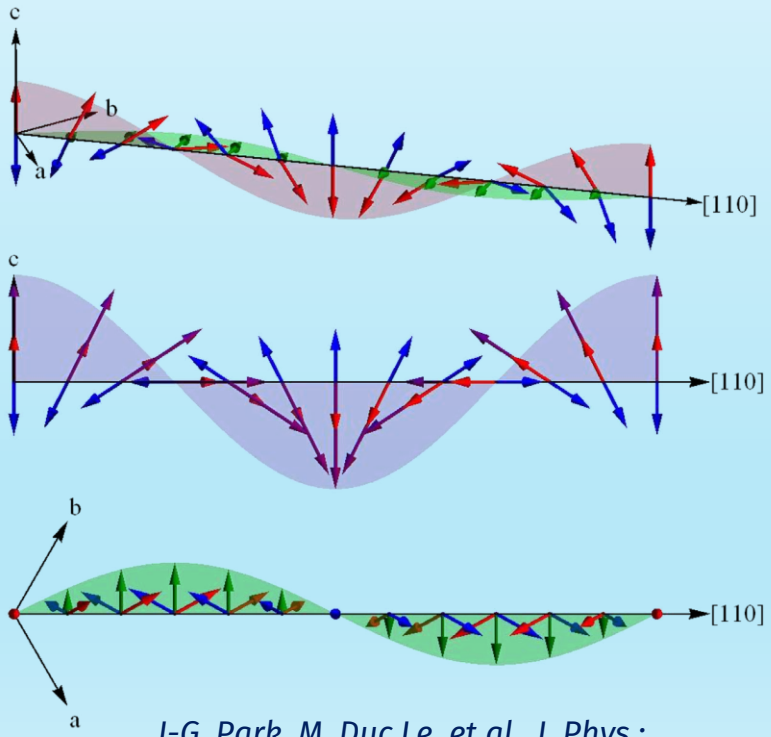

J-G. Park, M. Duc Le, et al., J. Phys.: Condens. Matter 26 (2014) 433202

BiFeO3 forms an R3c rhombohedral structure at RT. This structure is also usually described in a hexagonal or pseudocubic lattice setting.

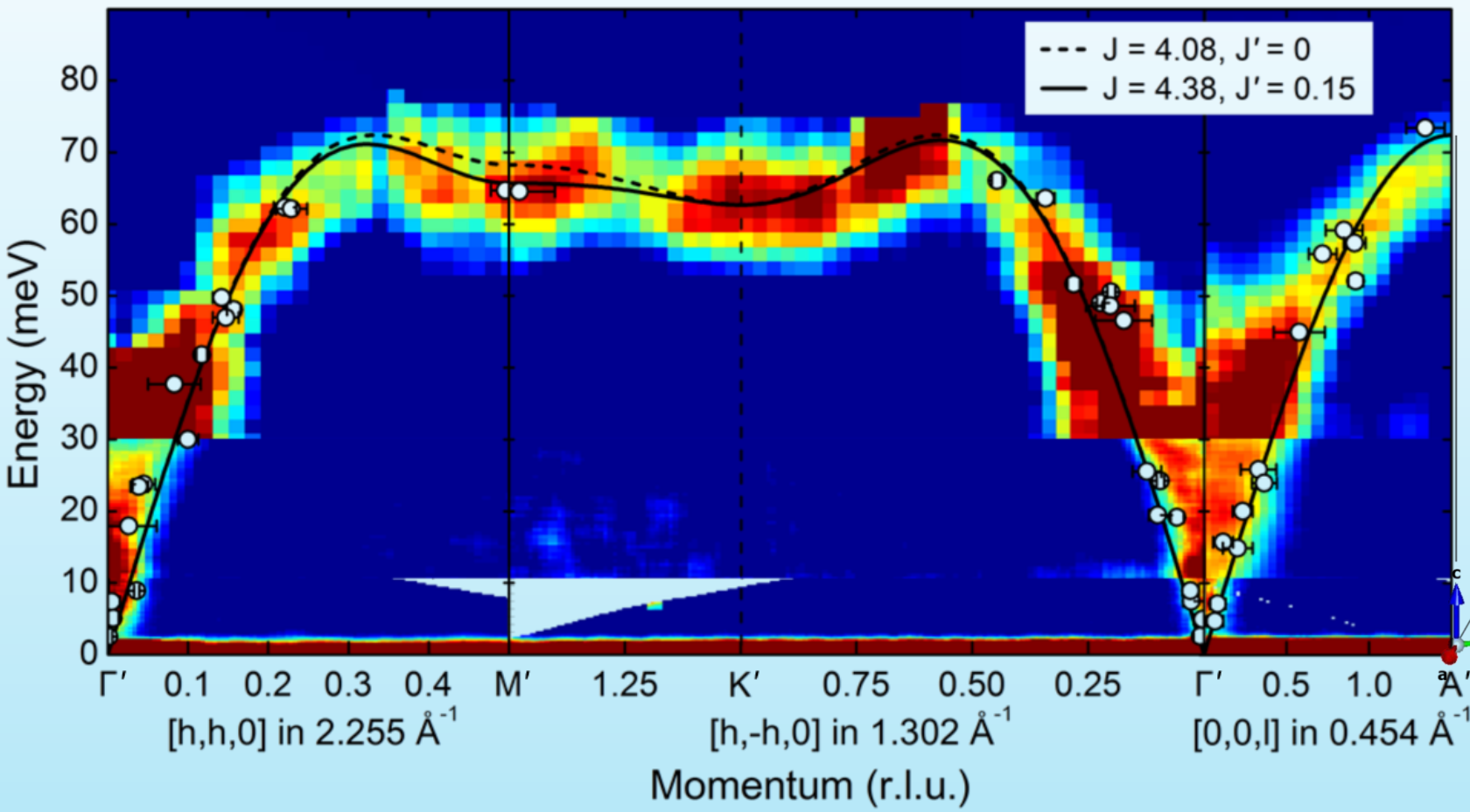

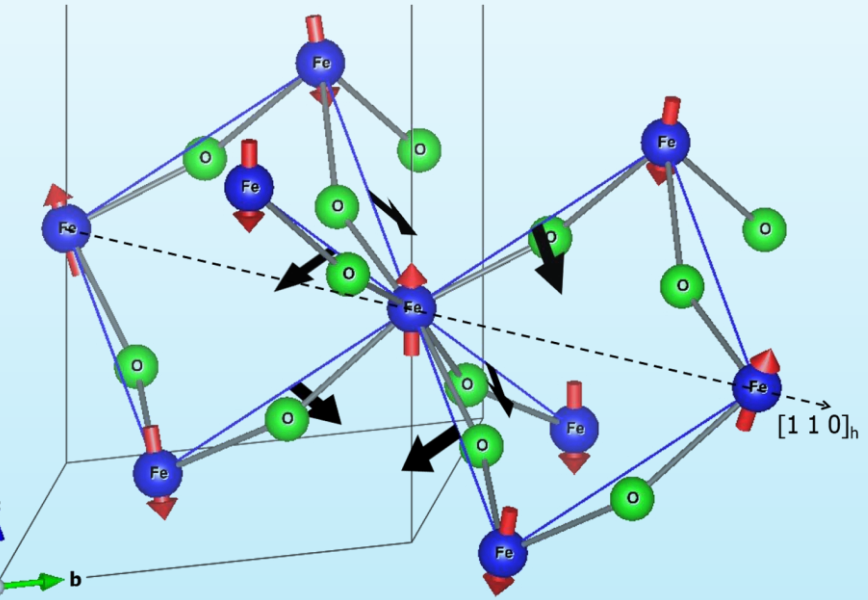

Full experimental magnon dispersion. The Dzyaloshinskii–Moriya vectors (black arrows) for nearest neighbours on distorted octahedra and part of the spin cycloid (red arrows).

J-G. Park, M. Duc Le, et al., J. Phys.: Condens. Matter 26 (2014) 433202

Scientific case:

$Mn_{1+x}V_{2-x}O_4$ and $Mn_{1-x}Co_xV_2O_4$ are frustrated magnets, attracting a lot of attention in both scientific and industrial fields due to their degenerate ground state, which gives rise to a exotic phenomena such as spin ices and spin liquids.

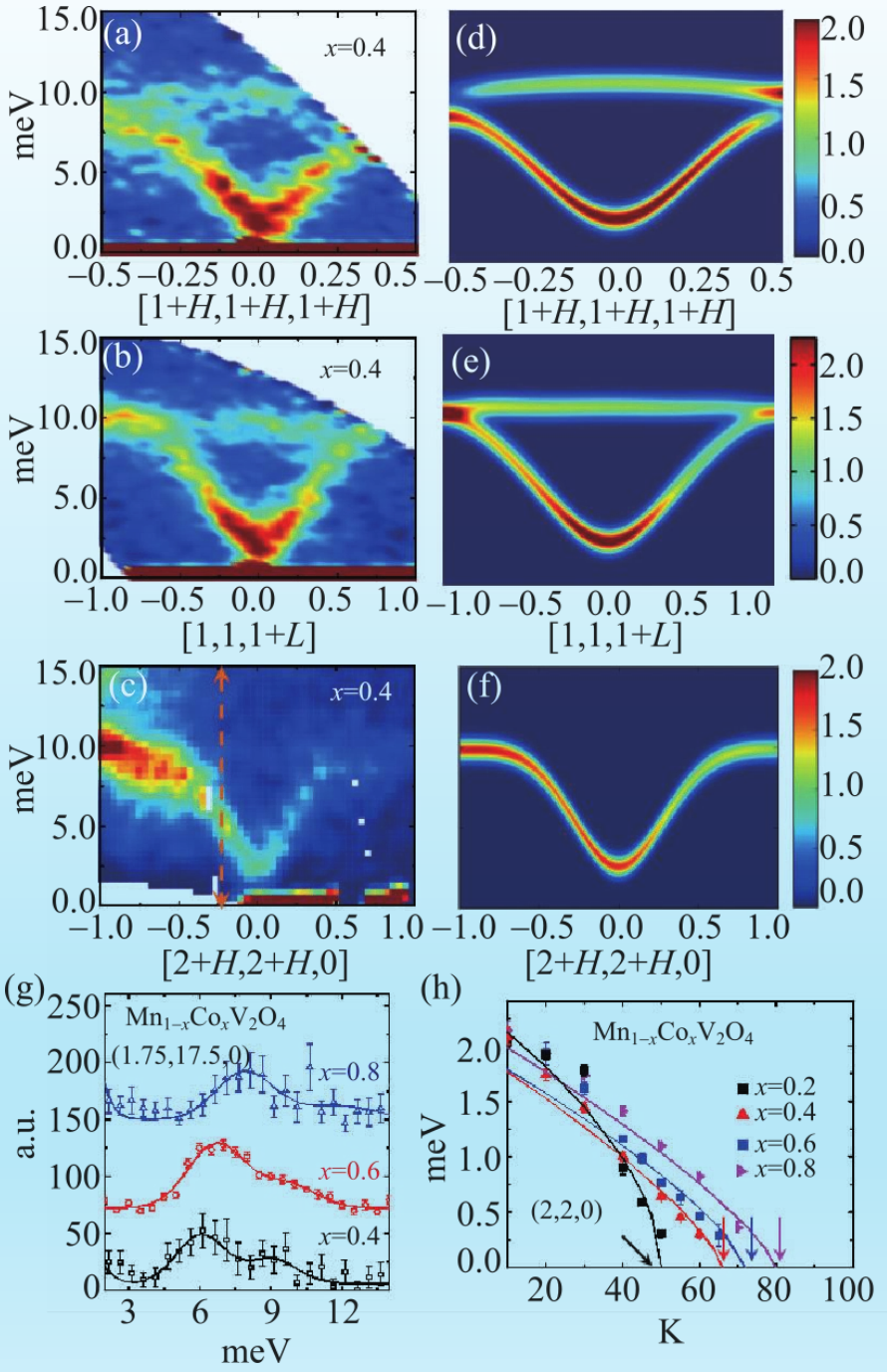

Inelastic neutron scattering magnetic excitation spectra of $Mn_{0.6}Co_{0.4}V_2O_4$ at 8 K. The arrow in (c) indicates the position of the constant Q value; (d-f) excitation spectra by equation; (g) At 8 K, the spin excitation spectrum at (1.75, 1.75, 0) varies with the sample composition. The solid line is the result of Gauss fitting; (h) The relationship between the spin wave energy gap at the centre of the magnetic region (220) and the temperature.

Examples: Small angle neutron scattering (SANS)

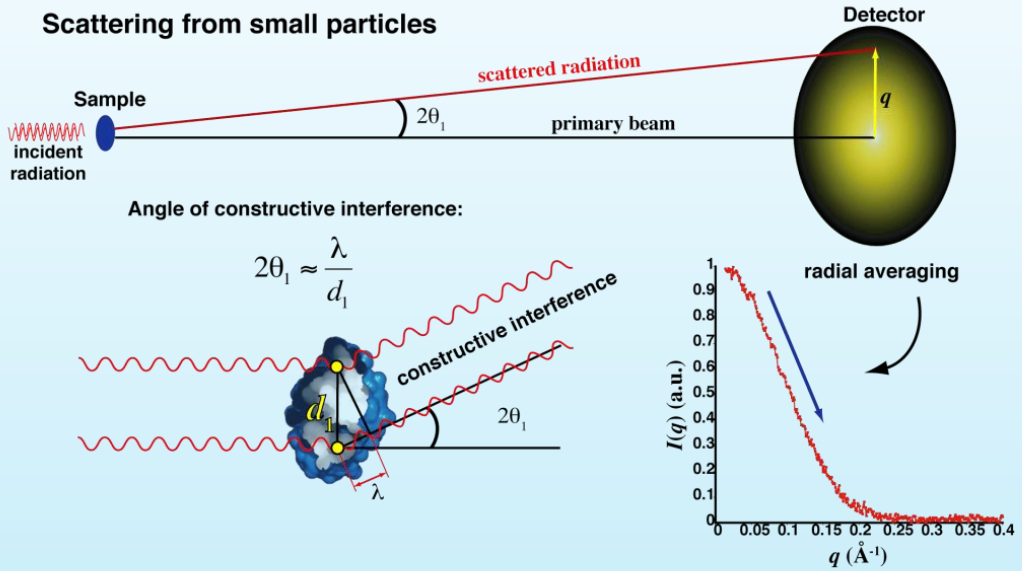

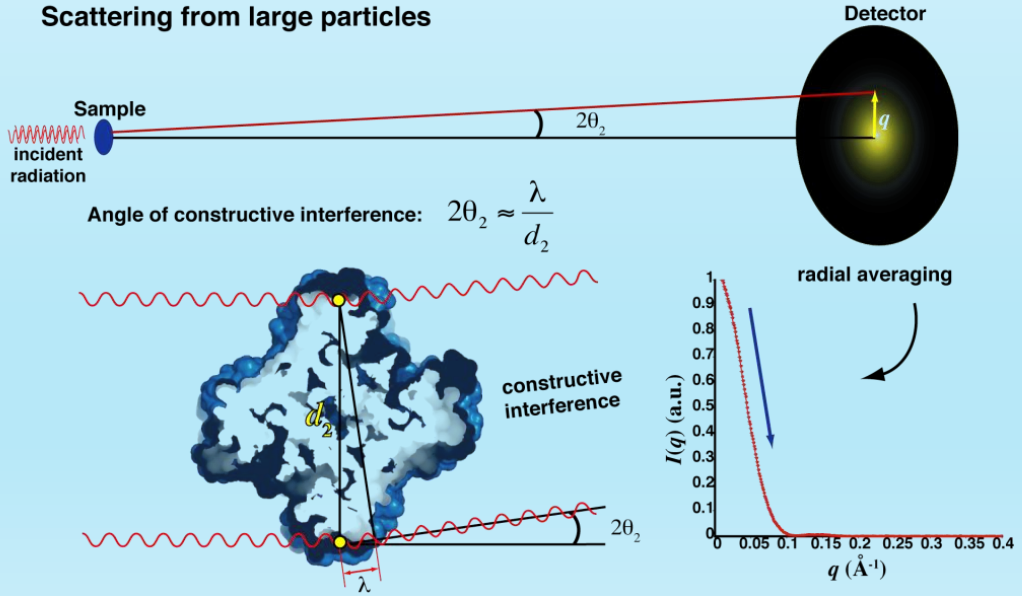

$$V^*(r) = \frac{2\pi\hbar^2}{m} b\delta(r)$$

Fermi pseudopotential

$$\rho(r) = \langle b_{coh} \rangle_{V \approx \frac{2\pi}{10Q}}$$

Scattering length density

$$\frac{\partial\sigma}{\partial\Omega}(Q) = N_p V_p^2 (\Delta\rho)^2 F(Q) S(Q) + B_{inc}$$

contrast factor — *form factor* — *sructure factor*

The angle for constructive interference is inversely proportional to the size of the scattering object.

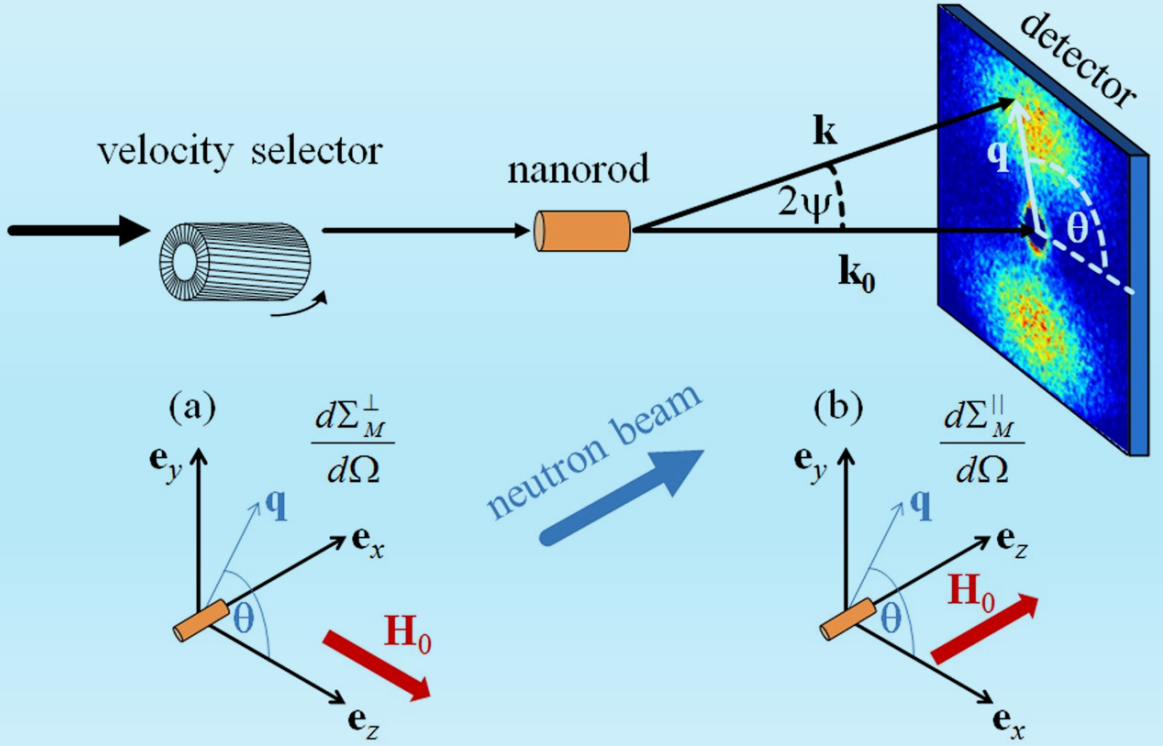

Scientific case:

Switchable or ‘smart’ thermoresponsive polymer hydrogels

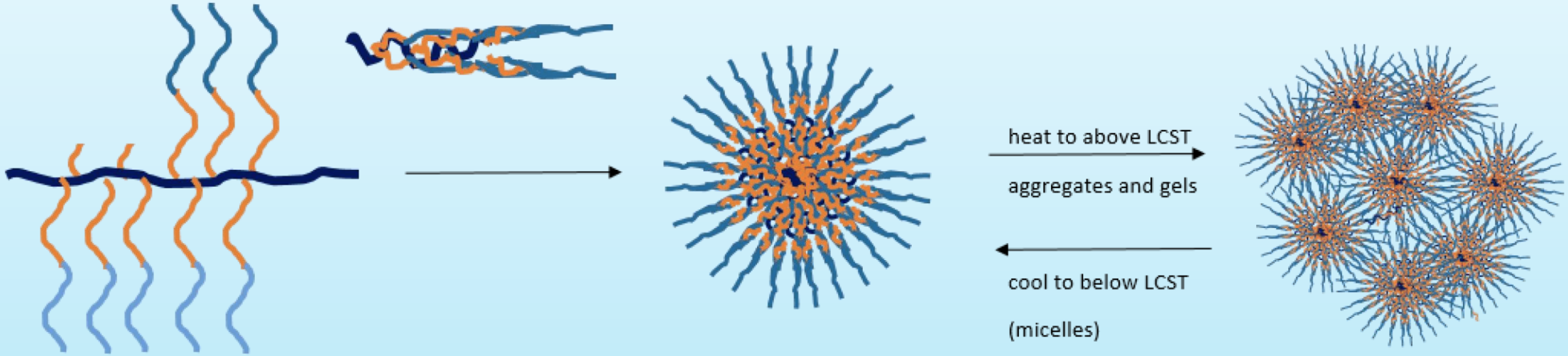

Thermoresponsive polymers in aqueous solution collapse from extended coils to compact globules when the temperature is raised above their cloud point (so called because the solution becomes turbid due to the formation of the aggregates), displaying lower critical solution temperature (LCST) behaviour, an effect that can be exploited by cross-linking the polymers. The switching time and reversibility are of great importance for applications such as controlled ultrafiltration. Time-resolved SANS provides a wealth of information on the structural changes at the cloud point.

Switchable or ‘smart’ thermoresponsive polymer hydrogels

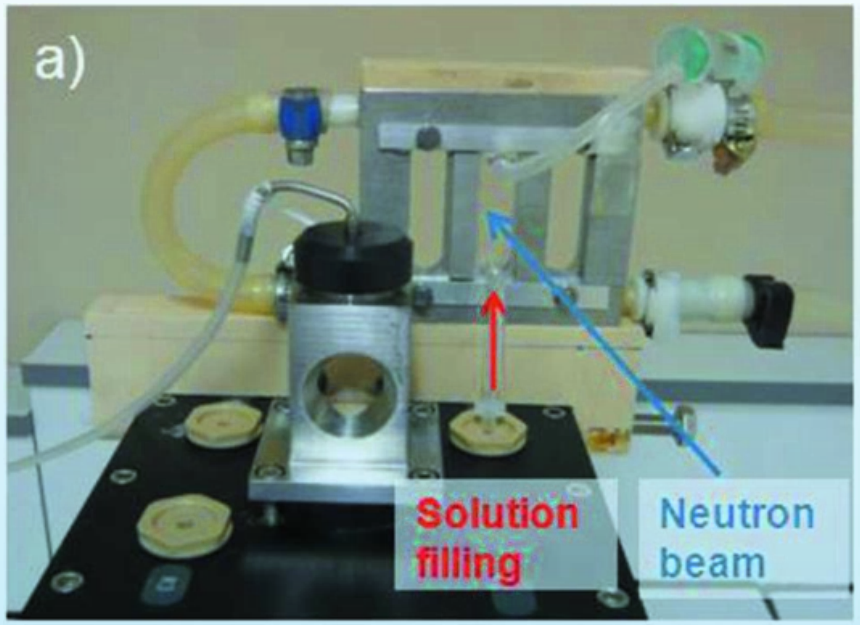

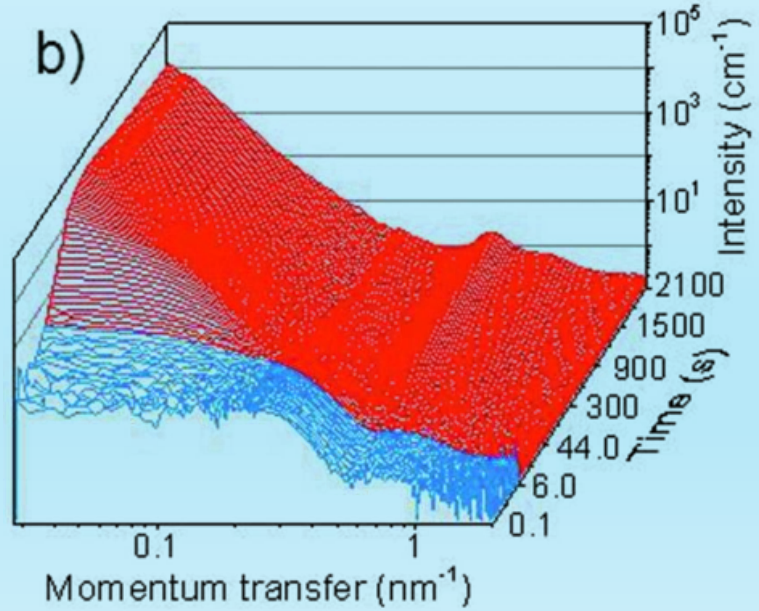

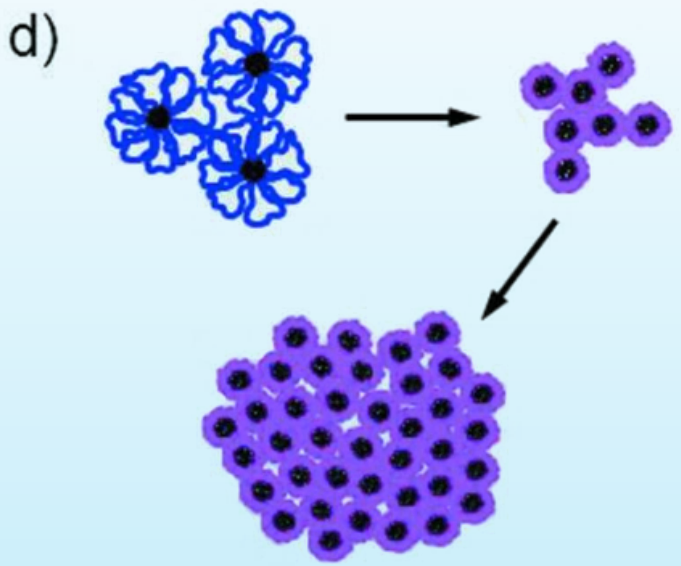

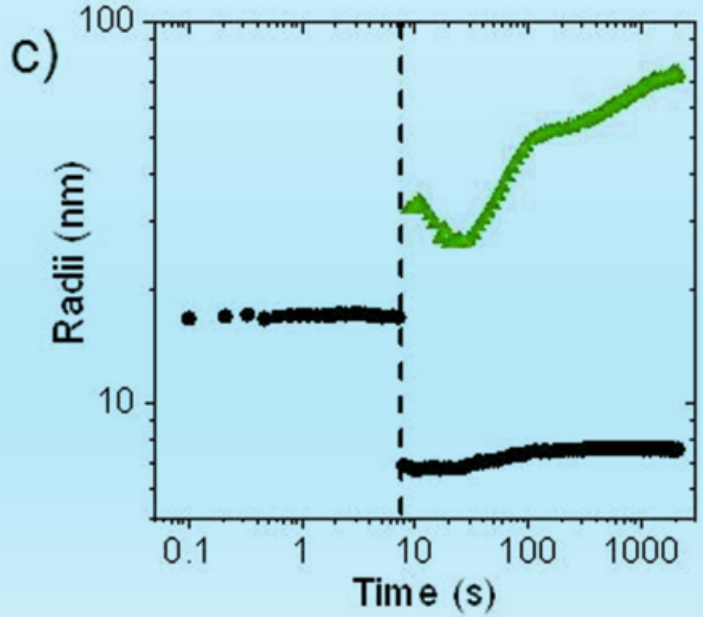

Time-resolved SANS during a temperature jump in a polymer solution.

(a) Modified stopped-flow instrument.

(b) SANS curves from a 200 mg ml^{-1} solution of polystyrene-block-poly(N-isopropylacrylamide)-block-polystyrene triblock copolymer with fully deuterated polystyrene blocks in D2O, for a temperature jump from 303 to 308 K. Temperatures below the cloud point (305.7 K) are shown in blue and above in red.

(c) Plot showing the radii of the micelles (black circles) and the aggregate size (green triangles) with time. The dashed line marks the cloud point.

(d) Schematic diagram of polymer collapse and aggregate formation.

*V.K. Peterson, C.M. Papadakis ., IUCrJ (2015). **2**, 292–304*

10 *Conclusion: the need for NS instrumentation dedicated for functional materials research*

Characterisation of functional materials, as e.g. in the study of electrode structure and lithium distribution involves powder diffraction and **total scattering**, reflectometry, neutron depth-profiling, Imaging, and more.

Traditional diffraction considers the long-range structure, whereas the **total scattering**, as implemented in the pair-distribution function (PDF), uses both Bragg and diffuse scattering and is sensitive to local environments.

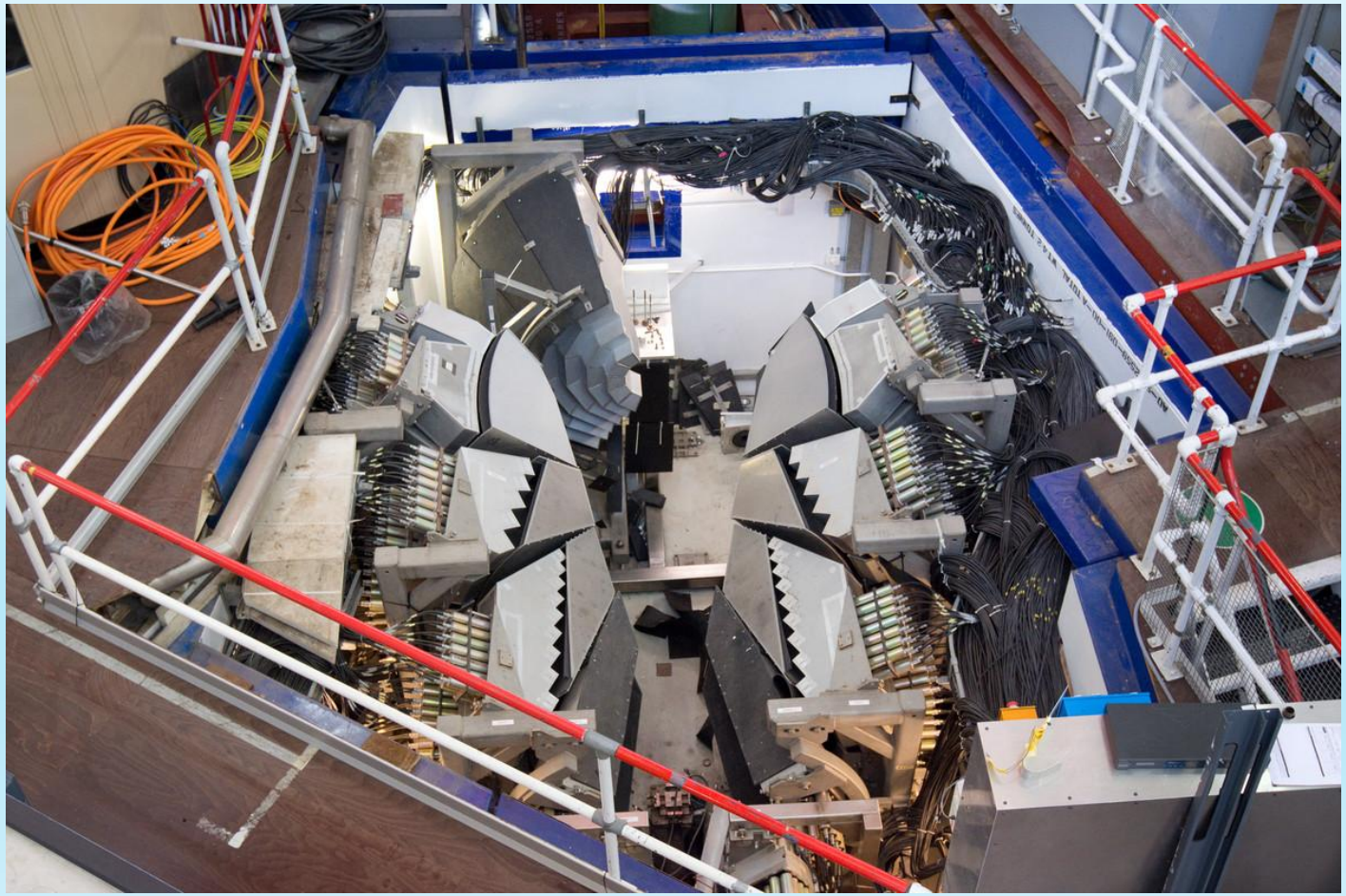

The General Materials Diffractometer (GEM) at ISIS Neutron and Muon Source (RAL) is used for high intensity, high resolution neutron diffraction and pair distribution function experiments to study the structure of crystalline powders and amorphous materials.

If we wish to understand and improve functional materials, it is paramount to understand the structure at all length scales and with sufficient time resolution to follow physical and chemical processes.

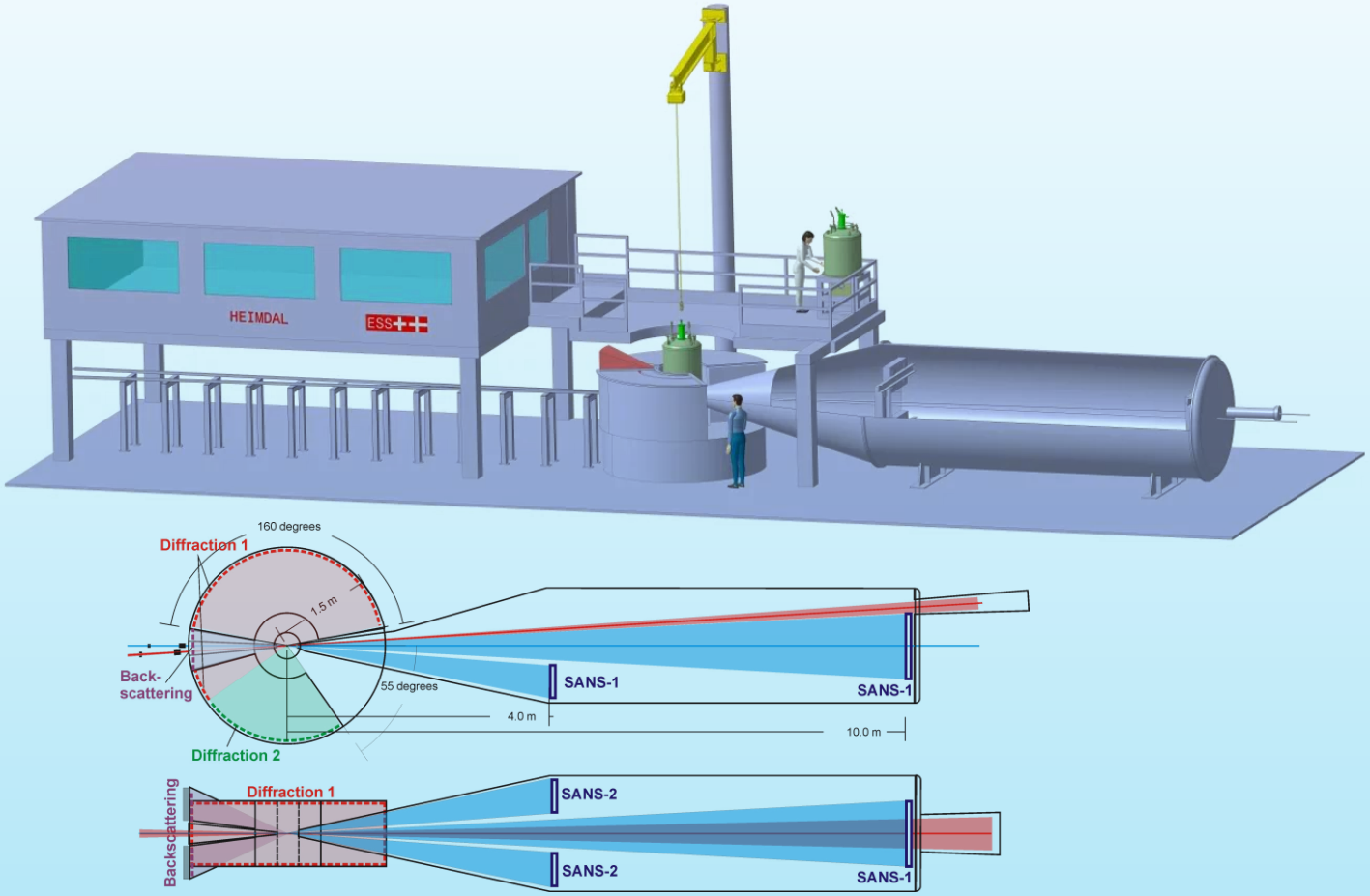

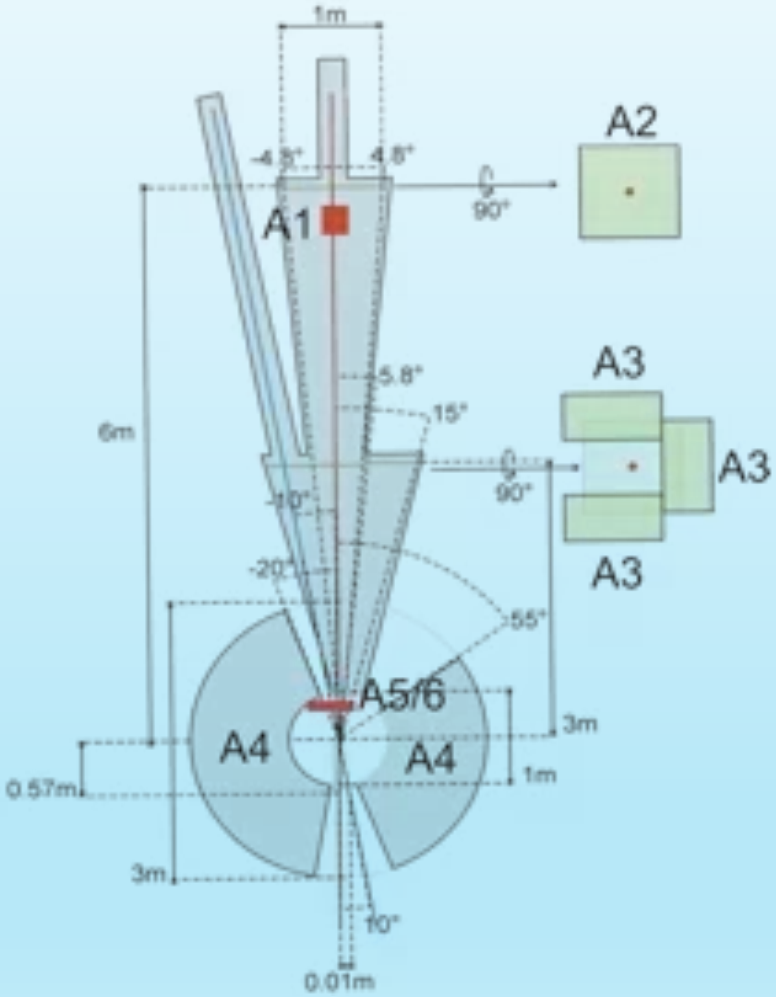

*HEIMDAL @ ESS will combine **NPD** (neutron powder diffraction), **SANS** (small angle neutron scattering) and **NI** (neutron imaging) in a single instrument allows studying multiple length scales simultaneously and obtaining information on the atomic-, nano-, meso-, and microstructure scale.*


Thank you for listening